BLOCH-ZENER OSCILLATIONS OF A COLD ATOM IN AN OPTICAL CAVITY

BLOCH-ZENER OSCILLATIONS OF A COLD ATOM IN AN OPTICAL CAVITY

By

PRASANNA VENKATESH BALASUBRAMANIAN, B.Sc.

A Thesis
Submitted to the School of Graduate Studies
in Partial Fulfillment of the Requirements
for the Degree
Master of Science

McMaster University

MASTER OF SCIENCE (2008) McMaster University
(Physics) Hamilton, Ontario

TITLE: Bloch-Zener Oscillations of a Cold Atom in an Optical Cavity

AUTHOR: Prasanna Venkatesh Balasubramanian, B.Sc.(Chennai Mathematical Institute)

SUPERVISOR: Dr. Duncan O'Dell

NUMBER OF PAGES: viii, 68

Abstract

A quantum particle moving in a periodic potential, with periodicity d, when acted by an external constant force F undergoes the dynamical phenomenon of Bloch-Zener oscillations (BZO) . We investigate BZO of a neutral cold atom in an optical cavity pumped by a laser. We find that the single mode electromagnetic field of the optical cavity is affected by the atomic dynamics and propose the idea that a measurement of the electromagnetic field leaking out of the cavity will reflect the BZO frequency $\omega_{\mathrm{B}} = Fd/\hbar$, and can be used for a precision measurement of F. The motivation for such a study comes from the fact that if the force F is gravity then one can probe gravitational forces on sub-millimeter scales since the size of these systems are generally a few hundreds of microns. Such a study can be used to detect deviations from Newtonian gravity at short range proposed by some theories beyond the standard model of particle physics.

Contents

List of Figures

List of Tables

Chapter 1

Introduction

When electrons in a crystal lattice with period d are subject to a constant force F, as in the case of an electric field, they undergo oscillatory motion. This idea was proposed by Zener in [1] based upon earlier work by Bloch [2], the frequency of these Bloch-Zener Oscillations (BZO) is given by :

$$\omega_{\mathrm{B}} = \frac{Fd}{\hbar} \ . \tag{1.1}$$

BZO have been proven difficult to observe in condensed matter systems since scattering from impurities leads to rapid dephasing. The first observations [3] were made in epitaxially grown semiconductor superlattices where DC electric fields were used to generate THz oscillations, but nevertheless dephasing occurs within several periods [4]. Cold atoms in optical lattices have provided an alternate setup to observe BZO. [5, 6].

With the discovery of laser cooling (proposed by [7], first experiments done by [8] followed by [9]) cooling atoms to temperatures as low as a few microKelvin became possible. At such low temperatures the quantum mechanical nature of the atom becomes important. Laser cooling combined with electromagnetic trapping leads to some spectacular quantum mechanical effects including Bose Einstein condensation [10, 11] of atoms where the atoms macroscopically occupy a single quantum state. Apart from the achievement of BECs, another interesting development was that atoms cooled to such low temperatures can then be held in optical lattices, which are standing waves made by the interference of two or more laser beams. Cold atoms in optical lattices are analogous to electrons in a periodic solid lattice. In this manner traditional condensed matter systems can be simulated using cold atoms. Although such cold atom systems are analogous to traditional condensed matter systems, they enjoy a significant number of advantages. Atoms in traps and lattices are extremely idealized systems with almost no imperfections or impurities and minimal interactions with the environment. They are therefore simple to describe theoretically and maintain their quantum coherence for long times in comparison to the relevant timescales

of the dynamics. In atomic systems almost all of the parameters are under our control. For example, the dimension and symmetry of the lattice, the strength and even the sign of the interatomic interactions, can all be chosen at will. The measurement schemes are radically different from traditional condensed matter schemes, e.g. single atoms can be non-destructively imaged, allowing us to track (and address) individual atoms in real time (see references [12]-[14] for some of the landmark experiments in this field and [15] for a comprehensive review of many-particle cold atom systems). Thus cold atoms can be used to study quantum mechanics in a setup that has just the bare essentials of the problem.

In the field of cavity quantum electrodynamics (QED) , the ability to study the interaction of single atoms withthe electromagnetic field inside a cavity has enabled the realisation of simple individual quantum systems whose dynamics can be manipulated (look at [16]-[21]). The availability of small cavities (length$\sim 10^2\,\mu$m) with very high finesse means that the coherent interaction between the electromagnetic mode in the cavity and the atom is strong and hence a single atom can significantly alter the field inside the cavity. This is because the atom-light coupling constant in the dipole limit, g_0, is inversely proportional to the square root of the cavity mode volume. In the so called strong-coupling limit sources of dissipation like spontaneous scattering and loss of light from imperfect mirrors (which is low for high finesse cavities) are much smaller than the coherent atom-light coupling g_0.

In this thesis, the system we consider is a single two-level cold-atom with resonance frequency ω_0 in an optical cavity. We assume that the electromagnetic field inside the cavity is a single-mode field with frequency ω_c and the atom-field interaction is in the dipole limit. The cavity has a linewidth κ and we drive the cavity mode on resonance using an external pump laser. The cavity frequency and the atomic levels are far detuned from each other. This means one can ignore the incoherent spontaneous emission process and the dipole force experienced by the atom can be derived from a potential that is periodic with period given by π/k_c (where $\omega_c = ck_c$). Thus, effectively we have a single atom moving in a periodic potential. We add to this a constant force term given by F. This means BZO of the atom will occur. We propose to use gravity as the force causing the BZO and make a precision measurement of $\omega_{\rm B}$, which in turn will determine F.

The motivation for a such a study arises because some theories beyond the standard model of particle physics [22, 23] that incorporate extra spatial dimensions predict that the form of Newton's law of gravitation may be modified at short ranges (denoted by R) i.e.

$$F = G_{\rm n}^{*}\frac{m_1 m_2}{r^{\rm n+2}} \text{ for } r \ll R \tag{1.2}$$

$$= G_{\rm n}^{*}\frac{m_1 m_2}{R^{\rm n} r^2} \text{ for } r \gg R \tag{1.3}$$

In the above equation the sub-script n stands for the number of extra-dimensions in the fundamental theory used to derive the modified Newton's law. Optical cavities with lengths on the order of hundreds of microns have been produced. The measurement of the force F using such a setup can help one probe force ranges on the micron scale and this can in turn help to test the validity of the above form for gravity. Moreover one can use such a setup to measure other short range forces like the Casimir-Polder force [30] or the local acceleration due to gravity g.

An important feature of our proposal concerns the measurement process. As mentioned before we assume that we are in the strong-coupling regime of cavity QED where the atom-field coupling g_0 is large. Hence the atomic dynamics affects the electromagnetic field inside the cavity. A simple way to understand this is to appeal to a classical model where a point-like atom is in a standing wave electromagnetic field that is heavily detuned from the atomic transition frequency. When the atom sits at a node of the cavity field, the dipole coupling is zero and the transmitted intensity is maximum and vice-versa for the antinode. Thus the transmitted intensity in a cavity depends on the atomic position. In other words the effective refractive index of the cavity considered as a black box is changed by the presence of the atom [20]. The presence of an atom effectively changes the resonance frequency of the cavity and the amplitude and phase of the transmitted light depends on atomic position.

The measurement process in this scheme involves observing the light that is transmitted through the cavity mirror which has finite reflectivity. We find from our analysis that the transmitted field's phase and amplitude are modulated at the Bloch frequency. Thus, a *continuous* measurement of the transmitted field can be used to determine the Bloch frequency. In BZO experiments using cold atoms [5, 6] [24]-[28] the general measurement procedure involves holding the atoms in an optical lattice for different times followed by a time of flight measurement where the atoms are destructively imaged. Hence to even measure one BZO many repetitions of the above process are needed. In contrast, for the scheme we propose, one can continuously observe many Bloch periods from the cavity output.

The plan of the thesis is as follows. In the second chapter we present the Hamiltonian for our problem and derive coupled equations of motion for the field and the atomic degrees of freedom. In the third chapter we detail the basic theory of BZO. In the fourth chapter the coupled equations of motion are solved numerically and two qualitatively different regimes for the solution are identified. We also present a self consistent solution for the light field amplitude as a function of time based on the theory of BZO considered in chapter 3. Note that we have not gone into experimental details of the setup we propose in this introduction. We devote chapter 5 to give a rough schematic for the proposed experiment. We also discuss the limitations of this proposal and the experimental challenges that may arise.

In that chapter for the sake of completeness and comparison we also go through various experiments that have already been done/proposed in connection with using BZOs of cold atoms to perform precision measurements. The last chapter summarizes our work.

Chapter 2

Hamiltonian and Equations of Motion

2.1 Introduction

The system under consideration is a two-level atom in a single quasi-mode of an optical cavity. The cavity mode is driven resonantly by an external pump laser. The cavity mode frequency is detuned from the atomic transition frequency. The atom-field interaction is treated in the dipole approximation and the rotating wave approximation. This means our hamiltonian will be an extension of the well known Jaynes-Cummings hamiltonian for the interaction between a two-level atom and a single mode field.

2.2 The Hamiltonian

The hamiltonian broadly consists of the following parts [31, 32, 33]

$$H = H_{atom} + H_{field} + H_{int} + H_{pump} \ . \tag{2.1}$$

Let us now write down the expressions for the individual parts. The atomic internal degrees of freedom of the atom consists of two-levels separated in energy by $\hbar\omega_0$ and this can be represented using the Pauli matrix σ_z. In this formalism the internal states are represented by spinors. The atom's external degrees of freedom contribute to the Hamiltonian through the kinetic energy term and through the energy of interaction with the constant force F.

$$H_{atom} = \frac{\hbar\omega_0}{2}\sigma_z + \frac{\hat{p}^2}{2M} + Fz \ . \tag{2.2}$$

The free field term describes the single mode electromagnetic field inside the optical cavity (with frequency ω_c) :

$$H_{field} = \hbar\omega_c \hat{a}^\dagger \hat{a} \ . \tag{2.3}$$

In the pumping term, η gives the pumping parameter (we assume the driving mode is a classical laser field). In terms of laser photon current (I_{ph}) from the driving laser and κ, $\eta = \sqrt{\kappa I_{ph}}$. The pump laser frequency is given by ω_p.

$$H_{pump} = \mathrm{i}\hbar\eta \left(\hat{a}^\dagger \mathrm{e}^{-\mathrm{i}\omega_p t} - \hat{a}\mathrm{e}^{\mathrm{i}\omega_p t} \right) . \tag{2.4}$$

The driving term can be derived from the following consideration. Consider the interaction between a single driving mode $\hat{b}$ and the cavity mode $\hat{a}$. The standard photon-number conserving interaction term between two single modes is given by :

$$H_{\mathrm{dr}} = i\hbar\hat{a}^\dagger\hat{b} - i\hbar\hat{a}\hat{b}^\dagger. \tag{2.5}$$

If we now assume that the driving mode is a classical mode described by constant amplitude η and with time dependent phase $e^{-i\omega_p t}$ [1], we get :

$$H_{\mathrm{dr}} = i\hbar\eta \left(\hat{a}^\dagger \mathrm{e}^{-i\omega_p t} - i\hbar\hat{a}\mathrm{e}^{i\omega_p t} \right) , \tag{2.6}$$

which is the driving term in Eq. 2.4.

Finally we need to write down the atom-field interaction in the dipole approximation and the rotating wave approximation. Let us first write down the form of the dipole interaction.

$$H_{int} = (-\vec{d} \cdot \hat{\epsilon}) E(z,t) \ . \tag{2.7}$$

Now in terms of the single mode annihilation and creation operators the field inside the cavity is given by :

$$E(z,t) = \sqrt{\frac{\hbar\omega_c}{2\epsilon_0 V}} \left(\hat{a} + \hat{a}^\dagger \right) \cos(k_c z) \ . \tag{2.8}$$

Now we can represent the dipole moment (assuming we can choose it to be real) as,

$$\vec{d} = \vec{\mu}(\sigma^+ + \sigma^-), \tag{2.9}$$

where the σ^+ and σ^- are the ladder operators for the atomic states i.e. the former excites the atom to the higher state from the lower state and the latter does the reverse. We chose the atomic quantisation axis such that the dipole constant g is real and can be written in

[1] We assume that the driving mode is in a coherent state that obeys $\hat{b} \mid b(0)\rangle = \eta \mid b(0)\rangle$

the form :

$$g = g_0 cos(k_c z) \ . \tag{2.10}$$

In the above equation the atom-light coupling constant g_0 is defined as :

$$g_0 = \mu \sqrt{\frac{\omega_c}{2\epsilon_0 V \hbar}} \ . \tag{2.11}$$

This leads to the following expression for the interaction term :

$$H_{int} = \hbar g (\hat{a} + \hat{a}^\dagger)(\sigma_+ + \sigma_-) \ . \tag{2.12}$$

Now in the absence of the interaction term the evolution of the operators is as follows :

$$a(t) = \hat{a}(0) \mathrm{e}^{-\mathrm{i}\omega_c t} \tag{2.13}$$

$$\sigma_+(t) = \sigma_+(0) \mathrm{e}^{\mathrm{i}\omega_0 t} \ . \tag{2.14}$$

Hence in the above expression for H_{int}, the terms $\hat{a}\sigma_-$ and $\hat{a}^\dagger\sigma_+$ (anti-resonant terms) evolve much faster than the other terms namely $\hat{a}\sigma_+$ and $\hat{a}^\dagger\sigma_-$ (resonant terms). For example :

$$\hat{a}\sigma_- \approx \mathrm{e}^{-\mathrm{i}(\omega_c+\omega_0)t} \tag{2.15}$$

$$\hat{a}^\dagger\sigma_- \approx \mathrm{e}^{\mathrm{i}(\omega_c-\omega_0)t} \ . \tag{2.16}$$

Obviously, in the above equations, near resonance, the second term evolves much more slowly than the first. The anti-resonant terms can be ignored (since they average to zero) provided we are near enough to resonance so that the detuning $\delta = (\omega_c - \omega_0)$ obeys $\delta << (\omega_c + \omega_0)$. Neglecting the anti-resonant terms (Rotating Wave Approximation) we have :

$$H_{int} = \hbar g \left(\hat{a}\sigma_+ + \hat{a}^\dagger \sigma_- \right) \ . \tag{2.17}$$

Accordingly the full Hamiltonian is (where we include a phenomenological decay term using the cavity line width κ which signifies the fact that the cavity mirrors have finite reflectivities) :

$$H = \frac{\hbar\omega_0}{2}\sigma_z + \frac{\hat{p}^2}{2M} + Mgz + \hbar\omega_c \hat{a}^\dagger \hat{a} + \hbar g \left(\hat{a}\sigma_+ + \hat{a}^\dagger\sigma_- \right) - \mathrm{i}\hbar\eta \left(\hat{a}\mathrm{e}^{\mathrm{i}\omega_p t} - \hat{a}^\dagger \mathrm{e}^{-\mathrm{i}\omega_p t} \right) - \mathrm{i}\hbar\kappa \hat{a}^\dagger \hat{a}. \tag{2.18}$$

In our system the atom-light detuning δ is set to be large leading to low saturation of the atomic transition. This means the excited state occupation probability for the atom is very

low. For a atom with dipole coupling g_0 and spontaneous line-width Γ, in a standing wave light detuned by δ (with a mean photon number $\bar{n}$), the fractional population of the excited state is given by [34] :

$$\sigma_{22} = \frac{s}{2(1+s)}, \tag{2.19}$$

where the saturation parameter s is given by :

$$s = \frac{2g_0^2\bar{n}}{\delta^2 + \frac{\Gamma^2}{4}}. \tag{2.20}$$

For $s \ll 1$ we can set the Pauli matrix $\sigma_z = -1$, signifying the fact that only the lower level is occupied (this is called the linear dipole approximation [35]). Before we carry out that change we will adiabatically eliminate the excited state so that Eq. 2.12 leads to an effective light-induced potential for the ground state of the atom. The details of the adiabatic elimination are worked out in the Appendix A. The effective Hamiltonian after the adiabatic elimination is :

$$H = \frac{\hbar\omega_0}{2}\sigma_z + \frac{\hat{p}^2}{2M} + Mgz + \hbar\omega_c\hat{a}^\dagger\hat{a} - \frac{\hbar g_0^2\cos^2(k_c z)\hat{a}^\dagger\hat{a}}{\delta}\sigma_z - \mathrm{i}\hbar\eta\left(\hat{a}\mathrm{e}^{\mathrm{i}\omega_p t} - \hat{a}^\dagger\mathrm{e}^{-\mathrm{i}\omega_p t}\right) - \mathrm{i}\hbar\kappa\hat{a}^\dagger\hat{a}. \tag{2.21}$$

To the above Hamiltonian we apply a unitary transformation with,

$$\hat{U} = \exp\left[\frac{\mathrm{i}t}{\hbar}\hbar\omega_p(\hat{a}^\dagger\hat{a} + 1/2\sigma_z)\right]$$

This transformation, in conjunction with the assumption that the cavity mode and pump mode are in resonance, will eliminate the free evolution terms in the hamiltonian and express it in a form where the emphasis will be on the atom-light interaction. Using the prescription stated in Eq. A.3 for unitary transformations we have the transformed hamiltonian (where $\Delta_c = \omega_c - \omega_p$ and $\Delta_0 = \omega_0 - \omega_p$) :

$$H' = \frac{\hbar\Delta_0}{2}\sigma_z + \frac{\hat{p}^2}{2M} + Mgz + \hbar\Delta_c\hat{a}^\dagger\hat{a} - \frac{\hbar g_0^2\cos^2(k_c z)\hat{a}^\dagger\hat{a}}{\delta}\sigma_z - \mathrm{i}\hbar\eta\left(\hat{a} - \hat{a}^\dagger\right) - \mathrm{i}\hbar\kappa\hat{a}^\dagger\hat{a}\ . \tag{2.22}$$

We assume that the bare cavity-driving laser detuning is zero. So $\omega_c = \omega_p$ and $\Delta_c = 0$. We also set $\sigma_z = -1$ for reasons stated before. Because of this the first term in H' becomes $-\frac{\hbar\Delta_0}{2}$, a constant that can be ignored for deriving equations of motion. So the hamiltonian becomes (dropping the primes in the notation for convenience) :

$$H = \frac{\hat{p}^2}{2M} + Mgz + \frac{\hbar g_0^2\cos^2(k_c z)\hat{a}^\dagger\hat{a}}{\delta} - \mathrm{i}\hbar\eta\left(\hat{a} - \hat{a}^\dagger\right) - \mathrm{i}\hbar\kappa\hat{a}^\dagger\hat{a}\ . \tag{2.23}$$

Let us now second-quantise the external atomic degrees of freedom. Call the second-quantised field operator $\hat{\Psi}(z)$; then the Hamiltonian can be rewritten as :

$$H = \frac{\hbar^2}{2M}\int \left|\nabla_z \hat{\Psi}\right|^2 dz + \frac{\hbar g_0^2}{\delta}\, a^\dagger a \int \left|\hat{\Psi}\right|^2 \cos^2(k_c z)\, dx + F\int \left|\hat{\Psi}\right|^2 z\, dz - \mathrm{i}\hbar\eta(a - a^\dagger) - \mathrm{i}\hbar\kappa a^\dagger a. \tag{2.24}$$

The equations of motion are :

$$\mathrm{i}\hbar\dot{\hat{\Psi}} = [\hat{\Psi}, H] \tag{2.25a}$$

$$\mathrm{i}\hbar\dot{\hat{a}} = [\hat{a}, H]\ . \tag{2.25b}$$

Since we have adiabatically eliminated the excited state, the field operator equation for $\hat{\Psi}$ reduces to an equation for the wave function Ψ. Let us also assume the field is in a coherent state with coherence parameter α. We get the equation for α from the operator equation for $\hat{a}$. Thus, the equations of motion are :

$$\mathrm{i}\hbar\,\dot{\Psi} \;=\; \left(-\frac{\hbar^2}{2M}\partial_z^2 + \frac{\hbar g_0^2\,\alpha^*\alpha}{\delta}\cos^2(k_c z) + Fz\right)\Psi \tag{2.26a}$$

$$\dot{\alpha} \;=\; -\mathrm{i}\frac{\alpha}{\delta}g^2(t) + \eta - \kappa\alpha\ , \tag{2.26b}$$

where the term representing atomic back action on the field is given by :

$$g^2(t) = g_0^2\int |\Psi|^2 \cos^2(k_c z)\, dz\ . \tag{2.27}$$

From the equation for the atomic wave function (Eq. 2.26a) one can see that it is the Schrödinger equation for a quantum particle moving in a periodic lattice under the influence of a constant force. The lattice depth, is a function of time and is given by :

$$s(t) = \frac{\hbar g_0^2\,\alpha^*(t)\alpha(t)}{\delta}\ . \tag{2.28}$$

The periodicity of the lattice is given by the $\cos^2(k_c z)$ term and it is π/k_c. Our aim is to start with an initial state for the field and the wave function and calculate the field parameter α as a function of time. As stated in the introduction the observable physical quantity, light that leaks out of the optical cavity, can be described by the same field parameter α up to a multiplicative constant determined by the reflectivity of the mirrors.

In the next chapter the basic theory of BZO is discussed, which will be used to interpret the numerical results in the following chapter.

Chapter 3

Bloch-Zener Oscillation Theory

3.1 Introduction

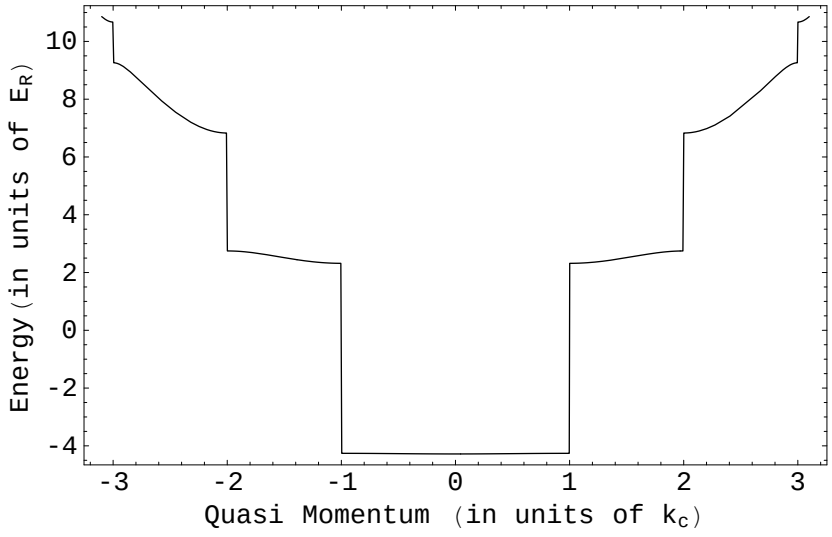

Figure 3.1: Band Structure in a deep lattice, hence the flat band structure(extended zone scheme).

In this chapter we will review the basic theory of Bloch-Zener oscillations. We will also look at what happens to this phenomenon when the lattice depth of the periodic potential in which the atom is moving is not constant in time. This extension to the standard theory of BZO is necessary because in an optical cavity in the strong coupling regime the motion of the atom causes the cavity resonance frequency to change with time which in turn controls the amount of light in the cavity.

3.2 Bloch Functions

As described in the last chapter the atomic wave function obeys a Schrödinger equation. Referring to Eq. 2.26a and Eq. 2.28, we write down the hamiltonian as :

$$H = H_0 + Fz \tag{3.1}$$

$$H_0 = \frac{\hat{p}^2}{2M} + V(z) = \frac{\hat{p}^2}{2M} + s\cos^2(k_c z) \ , \tag{3.2}$$

where the lattice depth is given by :

$$s \equiv \frac{\hbar g_0^2 \, \alpha^*(t)\alpha(t)}{\delta} \ . \tag{3.3}$$

In the above equation we have suppressed the time-dependence of the lattice depth s as one can notice. We will first consider the usual Bloch theory of a particle moving in a lattice with fixed depth.

The eigenvalue equation satisfied by H_0 is the well known Bloch equation first discussed for the case of an electron moving in the periodic potential of a crystal lattice. The periodicity of the lattice in our case is given by $V(z + \pi/k_c) = V(z)$. Bloch functions are indexed by two quantum numbers. The first is the band index. This comes into play since the energy levels of a particle in a periodic potential (Fig. 3.1) are arranged into bands. We suppress this index since we will be interested in a single band theory (only the ground band is of interest to us). The second index is the quasi-momentum index which is the analog of ordinary momentum, in periodic structures. Thus, the eigenvalue equation with ϕ_q representing the Bloch functions is :

$$H_0\phi_q = E_q\phi_q \ . \tag{3.4}$$

We next detail a few important properties of Bloch functions.

- *Defining Properties*

  Let us call the period of the lattice d where,

  $$d = \frac{\pi}{k_c} \ . \tag{3.5}$$

  Bloch functions can be written in the form (Bloch theorem [36])

  $$\phi_q(z) = e^{iqz}u_q(z) \ , \tag{3.6}$$

where the periodicity of u_q is given by :

$$u_q(z+d) = u_q(z) \ . \tag{3.7}$$

Another important property of the Bloch functions is :

$$\phi_{q+K} = \phi_q \ , \tag{3.8}$$

where K is a reciprocal lattice vector. K can take the following values :

$$K = 2n\frac{\pi}{d} = 2nk_c \text{ with } n \in \mathbb{Z} \ . \tag{3.9}$$

- *Born-Von Karmann Boundary Conditions*
  Lattices in the real world, although not infinite, are large in dimensions compared to the lattice spacing. This means we can impose periodic boundary conditions on the Bloch waves leading to discretization of the allowed quasi-momentum indices. Let us suppose that our system has a size $L = Nd = N\pi/k_c$. We require the Bloch functions to be periodic with this length :

$$\phi_q(z+Nd) = \phi_q(z) \ . \tag{3.10}$$

The periodic part of Bloch function, u_q, has the period d which means it is naturally periodic over integer multiples of d :

$$u_q(z+Nd) = u_q(z) \ . \tag{3.11}$$

In order to satisfy Eq. 3.10 we require :

$$\mathrm{e}^{\mathrm{i}qz} = \mathrm{e}^{\mathrm{i}qz+\mathrm{i}qNd} \tag{3.12a}$$

$$\mathrm{e}^{\mathrm{i}qN\pi/k_c} = 1 \ . \tag{3.12b}$$

The last condition implies :

$$Nq\pi/k_c = 2n\pi \text{ with } n \in \mathbb{Z} \ . \tag{3.13}$$

Thus, according to the BVK boundary conditions, the allowed values of q are :

$$q = q_n = 2nk_c/N \ . \tag{3.14}$$

This shows that the allowed values of q are discrete in a finite system.

In the next section we will discuss the theory of BZO.

3.3 Bloch-Zener Oscillation Theory

When we add a linear potential to the already existing periodic potential, we get the interesting dynamical phenomenon of Bloch-Zener oscillations [2, 1]. There are two ways to approach this problem. The first is to use semi-classical theory and the second is to use quantum mechanical theory. Although there was consensus on the semi-classical approach the quantum approach was intensely debated (for example look at references [39] - [42]). We take the view point of W.V. Houston expressed first in the reference [38].

The hamiltonian under consideration is:

$$H = H_0 + Mgz \ . \tag{3.15}$$

3.3.1 Semi-classical Theory

The first approach to understanding BZO is to use semi-classical theory. Here we assume that the quasi-momentum index q is a semi-classical variable which in the presence of a linear potential obeys the Bloch acceleration theorem [36]:

$$\hbar\dot{q} = -F \ . \tag{3.16}$$

This result originates from Sommerfeld's theory of electron transport in solids where the variable $\hbar q$ plays a role similar to that of regular classical momentum and the above equation is just Newton's second law with the force term $-F$. Solving the above equation, we get (with $q|_{t=0} = q_0$)

$$q(t) = q_0 - \frac{Ft}{\hbar} \tag{3.17}$$

Appealing to the Eq. 3.8, we can see that quasi-momentum indices that are separated by a reciprocal lattice vector $K = 2k_c$ can be identified. We see that the time evolution in Eq. 3.17 will eventually evolve q_0 to the edge of the first Brillouin zone i.e. near $q = k_c$, then we can map it back to the opposite edge of the zone $q = -k_c$. After this the quasi-momentum index evolves as before and in time T_B reaches the initial value of q_0, making this evolution periodic. To determine the period T_B set:

$$q(T_B) = q(0) - 2k_c = q(0) - \frac{FT_B}{\hbar} \ . \tag{3.18}$$

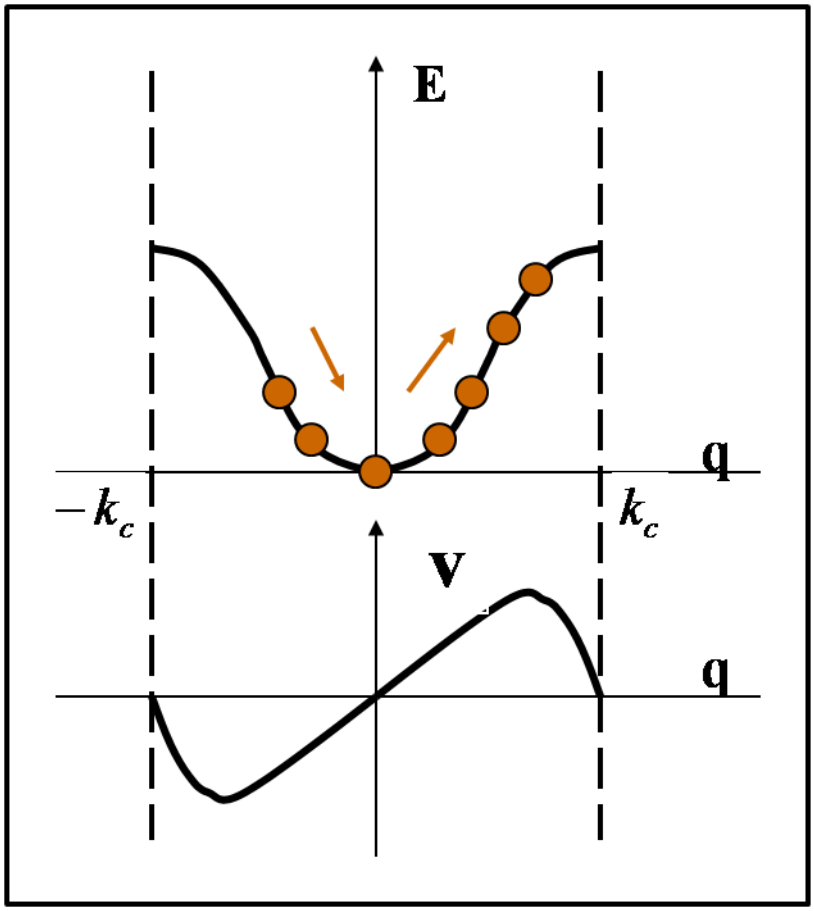

Figure 3.2: Schematic of Bloch evolution. In the first panel the energy dispersion of the ground band is shown. The second panel has the semiclassical velocity of the atom, $v \propto \frac{\partial E}{\partial q}$ which goes to zero at the band edges [44].

This determines the Bloch period and frequency as :

$$T_B = \frac{2\hbar k_c}{F} = \frac{2\pi\hbar}{Fd} \tag{3.19a}$$

$$\omega_B = \frac{Fd}{\hbar} \ . \tag{3.19b}$$

In Fig. 3.2 we plot the ground band dispersion and the semiclassical velocity ($v \propto \frac{\partial E}{\partial q}$) of a typical particle in a periodic potential. The velocity goes to zero at the band edge ($k = k_c$) and the atom re-emerges with a negative velocity at the opposite edge ($k = -k_c$) leading to the periodic BZO phenomenon. The change of sign of the velocity at the band edge can be thought of as Bragg scattering of the atom from the lattice potential.

Now we can substitute numerical values to check what the Bloch period will be for atoms used in cold atom setups. For Cs (M $\approx$ 132 amu) atoms in an optical lattice formed using

lasers with wavelength $\lambda_L = 785\,\mathrm{nm}$ [5],

$$\omega_B = Mg\pi/\hbar k_L \approx 8\,\mathrm{Khz}\ .$$

3.3.2 Quantum mechanical approach

Before going to the details of Houston's approach to the problem and writing down the wave function that bears his name, we will look at a simple way to understand the BZO phenomenon from quantum mechanical considerations. Consider the Schrödinger equation with the full hamiltonian :

$$i\hbar\frac{d\psi(z,t)}{dt} = (H_0 + Fz)\,\psi(z,t)\ . \tag{3.20}$$

With a gauge transform of the wave function $\tilde{\psi}(z,t) = \mathrm{e}^{-\mathrm{i}\frac{Ftz}{\hbar}}\psi(z,t)$, the equation of motion for $\tilde{\psi}$ becomes :

$$\tilde{H}\tilde{\psi}(z,t) = \left(\frac{(\hat{p}-Ft)^2}{2M} + s\cos^2(k_c z)\right)\tilde{\psi}(z,t) = \mathrm{i}\hbar\frac{d\tilde{\psi}(z,t)}{dt}\ . \tag{3.21}$$

Now the hamiltonian $\tilde{H}$ looks like H_0 except for the momentum term that is translated by Ft which implies the translation of the quasi-momentum index by $Ft/\hbar$. This is exactly the statement according to Bloch acceleration theorem (Eq. 3.17).

One important point that comes out of the Houston's work [38] and also the from the discussions of Zak and Wannier [39]-[42] is that it is difficult to find stationary eigenstate solutions for the full Hamiltonian $H = H_0 + Fz$. It has been established rigorously [43] that, in a finite lattice the solutions are resonances with finite widths rather than eigen-energies. Hence a simpler question to ask is whether there are solutions to the time-dependent Schrödinger equation Eq. 3.20 that also instantaneously satisfy the time-independent Schrödinger equation. The formulation of this question in the above manner suggests that the solution we find will be adiabatic in nature (since adiabatic eigenstate solutions to a time-dependent Hamiltonian have the same property, they are instantaneous eigenstates). This means we will get solutions that come with a limited regime of applicability.

Houston's solution is a direct extension of the semiclassical Bloch evolution idea. One way to motivate Houston's solution is to write down the eigenvalue equation obeyed by the spatially periodic "amplitude" part of the Bloch function u_q (Since we are concerned with just the ground band the eigen-functions are indexed only by the quasi-momentum index in this band) :

$$H_u u_q = \left(\left(\frac{(\hat{p}-\hbar q)^2}{2M}\right) + s\cos^2(k_c z)\right)u_q(z) = E_q u_q(z)\ . \tag{3.22}$$

Comparing this equation to the Hamiltonian for the Gauge transformed wave function of the full problem including the external force (i.e. compare H_u to $\tilde{H}$):

$$\tilde{H} = \left(\frac{(\hat{p} - Ft)^2}{2M} + s\cos^2(k_c z) \right) , \tag{3.23}$$

one can guess that the instantaneous eigenstate at time t for $\tilde{H}$ is [when you start with $\tilde{\psi}(z, t = 0) = \phi_{q_0}(z)$]:

$$\tilde{\psi}(z,t) = \mathrm{e}^{\mathrm{i}q_0 z} u_{(q_0 - \lambda t)}(z) \exp\left[-(\mathrm{i}/\hbar) \int^t E_{q_0 - \lambda\tau} d\tau \right] , \tag{3.24}$$

where $\lambda = F/\hbar$.

Thus the Houston solution for the full Schrödinger equation (Eq. 3.20) can be written as

$$\psi(z,t) = \mathrm{e}^{\frac{\mathrm{i}Ft}{\hbar}} \tilde{\psi}(z,t) = \exp\left[\mathrm{i}\left(q_0 - \lambda t\right) z\right] u_{(q_0 - \lambda t)}(z) \exp\left[-(\mathrm{i}/\hbar) \int^t E_{q_0 - \lambda\tau} d\tau \right] . \tag{3.25}$$

Naturally, this is not an exact solution. This choice satisfies the Schrödinger equation but for an extra term (call $q(t) = q_0 - \lambda t$)

$$-(\hbar/i) \left(-\lambda \frac{du_{q(t)}}{dq} \right) \exp\left[iq(t)z\right] \exp\left[-(i/\hbar) \int^t E_{q_0 - \lambda\tau} d\tau \right] \tag{3.26}$$

This term is zero when the external field $F = 0$ and/or when $\frac{du_{q(t)}}{dq}$ is small (this happens for example in the case of a free electron). In general Eq. 3.25 will be a good solution when the term Eq. 3.26 is small. This is true when the external field is small and we will quantify what we mean by small below. When the external field is small this solution is a good approximation to the exact solution for all q except at the edge of the band where $\frac{du_q}{dq}$ becomes large or undefined, so this needs to be handled carefully.

Qualitatively one can see that the wave function at the edge of the zone will be identical to the function at a point on the opposite end of the zone and we can think of the atom as Bragg reflecting. After this process the quasi-momentum wavevector continues to evolve in the same manner as before through the first Brillouin zone. When the electronic band structure is considered in the extended zone scheme (as shown in the Fig. 3.1) the second band corresponds to motion in the 2nd Brillouin zone and so on for higher bands. With a weak external field λ we do not get transitions between zones/bands and our Bragg scattering picture is a legitimate one.

To see exactly the effect of the higher bands one can try a solution that contains Bloch functions with quasi-momenta in all the zones. This leads to the adiabaticity criterion,

which has been worked out in Appendix B. Broadly speaking the main frequency in our problem ω_B, the Bloch frequency, goes as the strength of the linear force and must be less than the band frequencies. The exact expression for adiabaticity is (Eq. B.9) :

$$\hbar\omega_B << \frac{M\Delta_E^2 d}{\hbar^2 k_c} \ ,$$

where Δ_E is the band gap energy.

If we have a lattice depth that is not constant in time and we started at $t = 0$ with a Bloch state in the lowest band, we assert that the above Houston type solution with a time-dependent lattice depth will still be valid. The most important criteria for validity of such a solution is that the frequency of lattice depth modulation must be much smaller than the band gaps in order to preserve adiabaticity. Given this to be the case, the Bloch evolved quasi-momentum index $q(t) = q_0 - \lambda t$ is still a good quantum number for the problem (see [37] for a similar treatment in the case of AC forces) . Since we will use this idea later let us explictly write down the Houston solution for a modulated lattice, with the initial quasi-momentum index being $q|_{t=0} = q_0$,

$$\psi(z,t) = \exp\left[i\left(q_0 - \lambda t\right)z\right] u_{(q(t),s(t))}(z) \exp\left[-(i/\hbar)\int^t E_{(q(\tau),s(\tau))} d\tau\right] \tag{3.27}$$

In the above equation we have indexed the function u and the eigen-energy E by the time-dependent lattice depth $s(t) = \frac{\hbar g_0^2\, \alpha^*(t)\alpha(t)}{\delta}$ in addition to the usual indexing by the quasi-momentum q. This serves to differentiate it from Eq. 3.25, where the lattice depth was understood to be constant. One final remark that will complete this chapter and set the stage for the numerical results is the observation that in the above solution, based on Bloch evolution, not only the phase of the solution changes but also the periodic part u changes with time. This is important because in our numerical simulations we start with Bloch functions as the intial wave function and the main quantity of interest, the coupling $g^2(t)$ (Eq. 2.27), is independent of the phase and will not change if only the phase evolves. Consequently, the field inside the cavity does not change for very deep lattices and this affects the detection process. In the tight binding regime with deep lattices, the functions u do not evolve in time. We ensure that our lattice depths are not in this limit.

In the next chapter we describe our methods to solve the coupled equations of motion Eq. 2.26a and Eq. 2.26b.

Chapter 4

Solving the Coupled Equations

4.1 Introduction

In this chapter we will present methods to solve the coupled equations (Eq. 2.26a) and (Eq. 2.26b). We will identify two qualitatively different regimes based upon the value of the coupling constant $\frac{g_0^2}{\delta\kappa}$ and determine solutions in those regimes.

4.2 Numerical Solution — Setting up the Equations

The equations we want to solve are the coupled equations of motion derived earlier namely Eq. 2.26a and Eq. 2.26b,

$$\mathrm{i}\hbar\,\dot{\Psi} = \left(\frac{\hbar^2}{2M}\partial_z^2 + \frac{\hbar g_0^2\,\alpha^*\alpha}{\delta}\cos^2(k_c z) + Fz\right)\Psi \tag{2.26a}$$

$$\dot{\alpha} = -\mathrm{i}\frac{\alpha}{\delta}g^2(t) + \eta - \kappa\alpha\ . \tag{2.26b}$$

The basic idea is to start with a given $\Psi(0)$ and α at $t = 0$. With this we solve Eq. 2.26a between 0 and some small time interval Δt, we then use $\Psi(0 + \Delta t)$ in Eq. 2.26b to obtain $\alpha(0 + \Delta t)$ and repeat the process for the amount of time we want. When we solve the equations for small times, we assume the right hand sides have no time dependence. For instance in Eq. 2.26a, the right hand side has the term $\frac{\hbar g_0^2\alpha^*(t)\alpha(t)}{\delta}$ which is time-dependent. But we assume that α takes the constant value of $\alpha(t - \Delta t)$ of the previous iteration. In this manner we can generate the field parameter α as a function of time. Thus, in this approach we make the time-dependent coupled equations into time-independent equations over very small time intervals. The field equation Eq. 2.26b has a simple solution. The only non-trivial equation is the Schrödinger equation. We solve this by going into the Fourier space of the wave function Ψ.

Before we solve the Eq. 2.26a we will first rewrite the equation in a scaled dimensionless form, i.e. starting from,

$$\mathrm{i}\hbar\,\dot{\Psi}(z,t) \;=\; \left(\frac{\hbar^2}{2M}\partial_z^2 + \frac{\hbar g_0^2\,\alpha^*\alpha}{\delta}\cos^2(k_c z) + Fz\right)\Psi(z,t)\;, \tag{4.1}$$

set $k_c z = x$, scale the energies in the problem by the recoil energy $E_R = \frac{\hbar k_c^2}{2m}$ and time by the Bloch period i.e. let $\bar{t} = \frac{t}{T_B} = \frac{tFd}{2\pi\hbar}$. Now the equations take the form :

$$\left(-\frac{\partial^2}{\partial x^2} + c_1\alpha^*\alpha\cos^2(x) + c_2 x\right)\Psi(x,\bar{t}) = \mathrm{i}\frac{c_2}{2}\frac{\partial\Psi(x,\bar{t})}{\partial\bar{t}}\;. \tag{4.2}$$

where the new scaled parameters are given by $c_1 = \frac{\hbar g_0^2}{\delta E_R}$ and $c_2 = \frac{\hbar\omega_{\mathrm{B}}}{\pi E_R}$. In the numerical solution we assumed that $\delta < 0$ which means the cavity resonance frequency is red detuned from the atomic transition frequency.

Another thing we can settle before solving the above Schrödinger equation is to solve the field equation Eq. 2.26b with constant terms on the right,

$$\frac{d\alpha}{dt} = \frac{-\mathrm{i}ag^2}{\delta} + \eta - \kappa\alpha\;, \tag{4.3}$$

where $g^2(t) = g_0^2\int|\Psi|^2\cos^2(k_c z)dz$. We evaluate g^2 at $\bar{t}$ to make it time independent. The equation can be re-written as :

$$\frac{d\alpha}{\eta + \alpha(-\frac{\mathrm{i}g^2}{\delta} - \kappa)} = dt\;. \tag{4.4}$$

Integrating the last equation over a small time interval $\Delta\bar{t}$ get :

$$\int_{\alpha(\bar{t})}^{\alpha(\bar{t}+\Delta\bar{t})}\frac{d\alpha}{\eta + \alpha(-\frac{\mathrm{i}g^2}{\delta} - \kappa)} = \int_{\bar{t}}^{\bar{t}+\Delta\bar{t}} T_B d\bar{t'}\;. \tag{4.5}$$

Solving the last equation we get the value of the field at time instant $\bar{t}+\Delta\bar{t}$ when we know the wave function $\Psi(\bar{t})$ and consequently the function $g^2(\bar{t})$,

$$\alpha(\bar{t}+\Delta\bar{t}) = \frac{\eta}{\mathrm{i}\frac{g^2}{\delta} + \kappa} + \frac{\eta + \alpha(\bar{t})\left(-\mathrm{i}\frac{g^2}{\delta} - \kappa\right)}{-\mathrm{i}\frac{g^2}{\delta} - \kappa}\mathrm{e}^{\delta\bar{t}T_B}\;. \tag{4.6}$$

With the field equation settled we can proceed to solve the Schrödinger equation in momentum space. We assume that the system is in a finite box. Box lengths will be in units of one lattice constant (one period of the $\cos^2(x)$ potential) which is π in the scaled units. Since we are in a finite box, we will assume periodic boundary conditions for our momentum vectors

(known as Born-von Karman (BVK) conditions Eq. 3.14).

The equation to be solved numerically is, (from now on we will refer to the Bloch Period scaled time units $\bar{t} = t/T_B$ as t for notational convenience)

$$\left(-\frac{\partial^2}{\partial x^2} - \tilde{s}(t)\cos^2(x) + c_2 x\right)\Psi(x,t) = \mathrm{i}\frac{c_2}{2}\psi(x,\bar{t}) \ , \tag{4.7}$$

where $\tilde{s}(t) = -c1\alpha^*\alpha = \frac{\hbar g_0^2 \alpha^*(t)\alpha(t)}{|\delta|E_R}$ is the lattice depth $s(t)$ (defined in (Eq. 2.28)) scaled by the recoil energy E_R (up to a sign).

Let $L = N_0\pi$ denote the length of our box in position space. Thus the allowed momentum wavevectors (by the BVK boundary conditions) are integer multiples of $k_0 = 2\pi/L$. The length of one reciprocal lattice vector in this picture is:

$$K = 2\pi/d = 2\pi/\pi = 2 \ . \tag{4.8}$$

Before we expand our equation in momentum space we can simplify the momentum space equations if we do a particular transformation on the position space wave function. The transformation is:

$$\Psi(x,t) = \tilde{\Psi}(x,t)\exp(-\mathrm{i}\frac{c_2}{\frac{c_2}{2}}tx) = \tilde{\Psi}(x,t)\exp(-\mathrm{i}2tx) \ . \tag{4.9}$$

The equation satisfied by $\tilde{\Psi}$ is:

$$\left(-\tilde{s}(t)\cos^2(x) + (-\mathrm{i}\frac{\partial}{\partial x} - 2t)^2\right)\tilde{\Psi}(x,t) = \mathrm{i}\frac{c_2}{2}\tilde{\Psi}(x,t) \ . \tag{4.10}$$

Note that the above transformation is nothing but the gauge transformation with the force term introduced in the previous chapter (Eq. 3.21), although in scaled units. Expanding $\tilde{\Psi}(x,t)$ in momentum space and substituting into the Schrödinger equation we get,

$$\tilde{\Psi}(x,t) = \sum_n b_n(t)e^{\mathrm{i}nk_0x} \tag{4.11a}$$

$$b_m(t)(mk_0 - 2*t)^2 - \frac{\tilde{s}(t)}{4}(2b_m + b_{m-N_0} + b_{m+N_0}) = i\frac{c_2}{2}\frac{db_m}{dt} \ . \tag{4.11b}$$

Thus, given the set of momentum coefficients $b_m(t)$ and the value of $\tilde{s}(t)$, to get to $b_m(t+\Delta t)$ we have to only solve the above first order equation. Once we have $b_m(t+\Delta t)$, we use that to find $\alpha(t+\Delta t)$ and for this we need to calculate $g^2(t) = g_0^2\langle\cos(x)^2\rangle$. Express $g^2(t)$ in

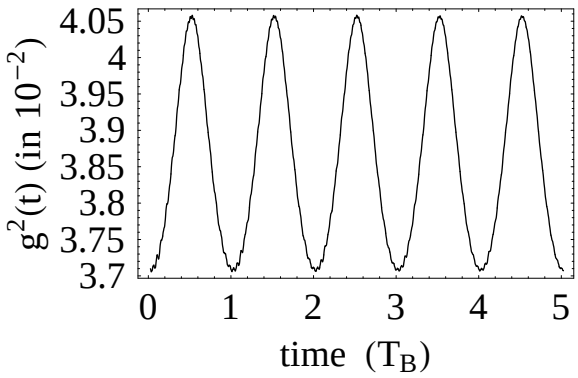

Figure 4.1: Coupling integral $g^2(t)$ as a function of time for $g_0^2/(\delta\kappa) = 0.05$, $\delta = -3.067 \times 10^{10}$ Hz, $\tilde{s} = 5$ and $\eta = 2.948 \times 10^6$ Hz.

terms of the momentum coefficients :

$$\langle \cos^2(x) \rangle = \sum_n \frac{|b_n|^2}{2} + \frac{1}{4} b_n^* (b_{n+N_0} + b_{n-N_0}) \ . \tag{4.12}$$

Before we go on to present the results of our numerical simulations, let us look at the parameters we chose for our simulations. In our model system we use the 780.2 nm transition line of Rb atoms in a cavity with decay width $\kappa = 2\pi \times 0.59$ MHz and the dipole coupling is $g_0 = 2\pi \times 12$ MHz (the cavity parameters and the dipole coupling parameter are taken from the reference [45]). The force term is the gravitational force given by $F = Mg$ where the acceleration due to gravity $g = 9.8\,\mathrm{ms}^{-2}$, giving $\omega_B = 5.289$ kHz.

In the next section we will see that the value of the parameter $g_0^2/(\delta\kappa)$ will lead to two qualitatively different regimes of the numerical solution. We will describe our solution in both these regimes. Note that from here on when we refer to the numerical value of $g_0^2/(\delta\kappa)$ we mean the positive absolute value.

4.3 Phase Regime

Consider equation Eq. 2.26b :

$$\dot{\alpha} \ = \ -\mathrm{i}\frac{\alpha}{\delta} g^2(t) + \eta - \kappa\alpha \ . \tag{2.23b}$$

The steady state solution for α can be got by setting $\frac{d\alpha}{dt} = 0$:

$$\alpha = \frac{\eta}{\kappa} \frac{1}{1 + \mathrm{i}\frac{g^2(t)}{\delta\kappa}} \ . \tag{4.13}$$

This solution is a good approximation to the real solution when the field relaxation time $\tau_a \approx \kappa^{-1}$ is much faster than the atomic dynamics. The atomic dynamics are characterised by frequencies such as the Bloch frequency, the band splitting in the periodic potential and $\omega_{\rm ho} = 2g_0|a|\sqrt{E_R/(\hbar|\delta|)}$ which is the effective harmonic frequency at the bottom of the wells. In deep lattices the band splitting tends to $\omega_{\rm ho}$, because each well of the lattice can be thought of as an independent harmonic oscillator potential. In typical experiments $\omega_{\rm B}$ and $\omega_{\rm ho}$ are of the order of $2\pi \times 10^3 s^{-1}$ whereas κ is in the range $2\pi \times 10^6 - 10^{10} s^{-1}$. Thus the steady state solution, which we use in our analytic calculations and general arguments, is a very good approximation although we solve the equation in full for our numerical calculations (Eq. 4.6). In conventional cavity QED, very high finesse cavities are used to reach high atom-photon coupling g_0, but in our case the cavity line width is the relaxation parameter and a very small κ is not ideal for this proposal.

The strength of the coupling term $g^2(t)$, that is defined in the equation Eq. 2.27, goes as g_0^2 where g_0 is the dipole coupling. Thus the important parameter in the above solution is the coupling value $\frac{g_0^2}{\delta\kappa}$. When this coupling value is very small, we can do the following. Expand the denominator of Eq. 4.13 :

$$\alpha \approx \frac{\eta}{\kappa}\left(1 - \mathrm{i}\frac{g^2(t)}{\delta\kappa}\right) \ . \tag{4.14}$$

The last equation can be thought of as the first order expansion of :

$$\alpha = \frac{\eta}{\kappa} e^{-\mathrm{i}\phi(t)} \ , \tag{4.15}$$

where

$$\phi(t) = \frac{g^2(t)}{\delta\kappa} \ . \tag{4.16}$$

Thus for a small value of the coupling, the amplitude of the light-field inside the cavity is unchanged and only the phase depends on time. We need to determine the form of $g^2(t)$ as a function of time. Before going to the quantitative results, the important feature we find is that the coupling $g^2(t)$ is a periodic function with the period T_B. Thus a continuous measurement of the light field phase in this regime, using for example a homodyne scheme, will determine T_B accurately. In a homodyne measurement apparatus (Fig. 4.2), the light field coming out of the cavity is combined with an intense local oscillator (LO) at a beam-splitter, and a detector collects the resulting interference signal. The relative phase, which we expect to be periodically modulated in time, can then be obtained by measuring the resulting intensity which is phase dependent.

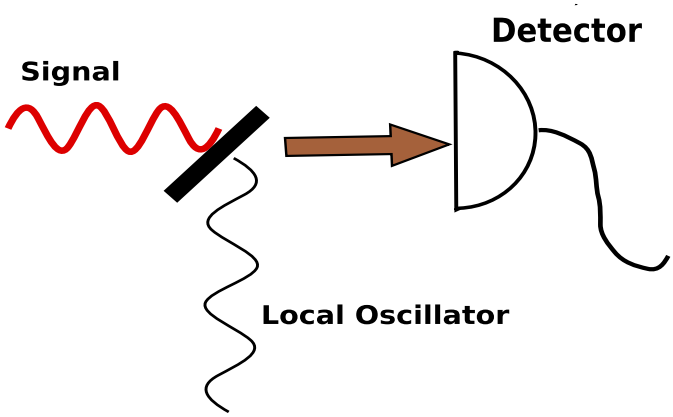

Figure 4.2: Adaptive Homodyne Measurement Schematic.

In our numerical simulation for this 'phase' regime we chose the coupling value $g_0^2/(\delta\kappa) = 0.05$. The values of g_0 and κ are those stated at the end of the last section and the value of coupling fixes the value of detuning ($\delta = -3.067 \times 10^{10}$ Hz). The next choice we make is the value of the initial lattice depth $\tilde{s}(0) = \frac{\hbar g_0^2 \alpha^* \alpha}{|\delta| E_R}$. A very deep lattice will mean that the linear force term will have a very small impact on the dynamics of the wave function. Motion within a lattice site (known as intrawell oscillations in semiconductor superlattice literature) will dominate BZO which are phenomena connected to coherence between different wells [49]. If the lattice depth is chosen to be very small the dynamics are dominated by the linear force and Landau-Zener tunneling dominates over BZO. We have from our simulations determined a range of $\tilde{s}$ where we can measure Bloch dynamics clearly. Hence in all our simulations we chose $4 < \tilde{s} < 15$. For the specific case of this phase regime simulation we use $\tilde{s} = 5$. From the expression for the lattice depth this determines the initial field parameter (assumed real), $\alpha_i = 0.7952$. We assume that this field is the empty cavity field given by $a_i = \frac{\eta}{\kappa}$ which determines $\eta = 2.948 \times 10^6$ Hz. This determines all the parameters that are needed for the simulation. We chose our initial wave function to be a Bloch function with quasi-momentum index $q = 0$ in the initial lattice depth $\tilde{s}(0)$. The coupling integral $g^2(t)$ was calculated and has been plotted in Fig. 4.1. Thus, we see that the phase is modulated at the Bloch frequency for small values of $g_0^2/(\delta\kappa)$.

4.4 Amplitude Modulation —— Larger Coupling Values

For larger values of $g_0^2/(\delta\kappa)$, the phase approximation made in the last section does not hold good. The amplitude of the field parameter, not just its phase, is affected. This means that the lattice depth $\tilde{s}(t) = \frac{\hbar g_0^2 \alpha^*(t)\alpha(t)}{|\delta| E_R}$ will be a function of time. In the results that we

discuss below we are assuming that the average intra-cavity photon number $\alpha^*\alpha$, which is directly proportional to the lattice depth, is the observable that will be measured from the signal that comes out of the cavity. Hence the aim of the simulations will be to look at the behaviour of lattice depth $\tilde{s}$ as a function of time. The simulations were done using $MATLAB^{®}$ [46] and a package for sparse matrix exponentials Expokit [47]. Figures were drawn using *Mathematica*® [48].

The first value of coupling we look at will be $g_0^2/(\delta\kappa) = 0.1$. This fixes, $\delta = -1.53 \times 10^{10}$ Hz. We choose our initial lattice depth to be given by $\tilde{s}(0) = 5.495$. As we have discussed above this fixes the value of the initial field amplitude, and this time we find $\alpha_i = 0.5912$ and hence the value of $\eta = 2.19 \times 10^6$ Hz. We again start with a Bloch state in the initial lattice depth with quasi-momentum index $q = 0$. The lattice depth as a function of time has been plotted in Fig. 4.3.

Since the square of the cavity field amplitude is directly proportional to the lattice depth i.e. $\tilde{s}(t) = \frac{\hbar g_0^2 |\alpha(t)|^2}{|\delta| E_R}$ we will throughout this section use the terms cavity field amplitude and lattice depth interchangeably in the discussion. Looking at the Fig. 4.3, one can see that for very short times the cavity field amplitude jumps from its atom-free initial value ($\alpha_i = \eta/\kappa$) to its steady state value in the presence of the atom. This jump can be understood from the steady state solution Eq. 4.13 i.e.

$$\alpha_i = \frac{\eta}{\kappa} \frac{1}{1 - i\frac{g^2(t)}{\delta\kappa}} \ .$$

The atomic coupling term in the denominator causes the jump and the subsequent dynam-

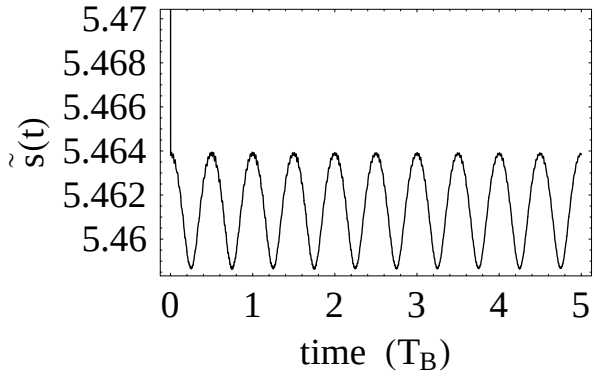

Figure 4.3: Lattice depth as a function of time for $\frac{g_0^2}{\delta\kappa} = 0.1$, $\delta = -1.53 \times 10^{10}$ Hz and $\eta = 2.19 \times 10^6$ Hz.

ics. After this initial jump the field amplitude is modulated at the Bloch frequency. Thus detecting the field amplitude as a function of time will lead to an accurate measurement of the Bloch period. One can see from the short time scale over which the initial jump happens

that it is a non-adiabatic change caused by particular assumptions of our initial state. So this jump from the initial value is transient in nature. We will also see in our considerations of larger coupling the fact that the initial transients are more pronounced and the initial jump will be much larger.

The next step is to examine if we can explain the modulation of our lattice depth from the Bloch acceleration theorem. We are still in parameter regimes where $\kappa > (\omega_{\mathrm{B}}, \omega_{\mathrm{ho}})$ and hence we can use the steady state solution for $\alpha(t)$ (Eq. 4.13) , which means :

$$\tilde{s}(t) = \frac{\hbar g_0^2}{|\delta| E_R} \frac{\eta^2}{\kappa^2} \frac{1}{1 + \left(\frac{g^2(t)}{\delta\kappa}\right)^2} \ . \tag{4.17}$$

Note that $\tilde{s}(t)$ appears explicitly on the left hand side of Eq. 4.17 and implicitly on the right hand side through the coupling integral $g^2(t)$. We need to solve this equation in a self-consistent manner. In order to help us understand Eq. 4.17 let us temporarily assume that the lattice depth is a given periodic function of time (for e.g. $s(t) = s_0 \sin(\omega_s t)$) rather than something that needs to be determined self-consistently. Let us also assume that the frequency $\omega_s \approx \omega_{\mathrm{B}}$ (this can be motivated from the full numerical solution discussed above). This means we can invoke the adiabaticity conditions introduced while discussing BZO in an amplitude modulated lattice at the end of section 3.3. Therefore, the adiabatic Houston solution for the modulated lattice introduced in section 3.3 (Eq. 3.27) is a valid solution to our problem. The idea then is to use the Houston solution to evaluate the coupling integral $g^2(t)$ at a given instant of time and then use it to solve Eq. 4.17 in a self-consistent manner for the lattice depth $\tilde{s}(t)$.

The Houston solution is given by :

$$\psi(z,t) = \exp\left[\mathrm{i}\left(q_0 - \lambda t\right) z\right] u_{(q(t),s(t))}(z) \exp\left[-(\mathrm{i}/\hbar) \int^t E_{(q(\tau),s(\tau))} d\tau\right] \ .$$

In our case the initial quasi-momentum $q_0 = 0$. Another important thing to note is that the self-consistent solution can only be found at discrete instants of time decided by the Born-Von Karman boundary conditions, because in calculating the self-consistent solution we use the Bloch evolved quasi-momentum vector:

$$q(t) = q_0 - 2t \ . \tag{4.18}$$

$q(t)$ must still be an allowed wavenumber by Born-Von Karman boundary conditions, which

means we have the BVK conditions for $q(t)$ and q_0 :

$$q_0 = m2\pi/L \tag{4.19a}$$

$$q(t) = m^{'}2\pi/L \ . \tag{4.19b}$$

Combining the above equations the allowed discrete time instants at which we calculate the self-consistent solution are :

$$t = (m - m^{'})\pi/L \text{ with } m, m^{'} \in \mathbb{Z} \ . \tag{4.20}$$

We solve equation Eq. 4.17 only at such allowed value of t.

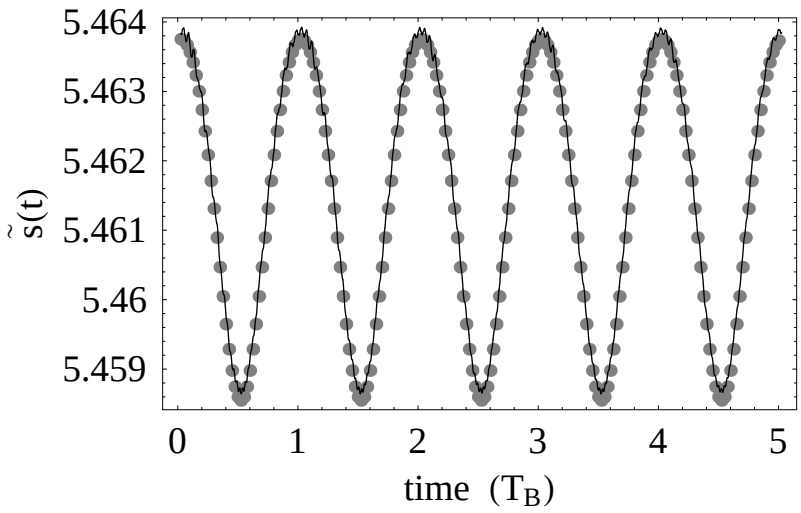

Figure 4.4: Lattice depth as a function of time for $\frac{g_0^2}{\delta\kappa} = 0.1$ compared to the self-consistent solution. The self-consistent solution is represented by the dots and the continuous line is the full numerical solution. Other system parameters are same as the ones used in Fig. 4.3. The self-consistent and full numerical solution are in good agreement.

This self-consistent solution for the lattice depth only needs to be evaluated over one Bloch period since it is periodic by definition. In Fig. 4.4 the self-consistent solution is compared to the settled down part of the numerical solution (the dots on the picture represent the self-consistent solution). We see that the numerical solution and the self-consistent solution are in close agreement.

The next coupling value we consider is $g_0^2/\left(\delta\kappa\right) = 0.5$. We choose the initial lattice depth $\tilde{s}(0) = 5.526$. This sets the following parameters, $\delta = -3.07\times10^9$ Hz, $\alpha(t=0) = \alpha_i = 0.2644$ and assuming the initial field is given by η/κ we get, $\eta = 9.8\times10^5$ Hz. With this setting we start with a Bloch state in the initial lattice depth and we have plotted the lattice depth as a function of time in Fig. 4.5.

As we had mentioned earlier we see that the transients at the beginning of the time

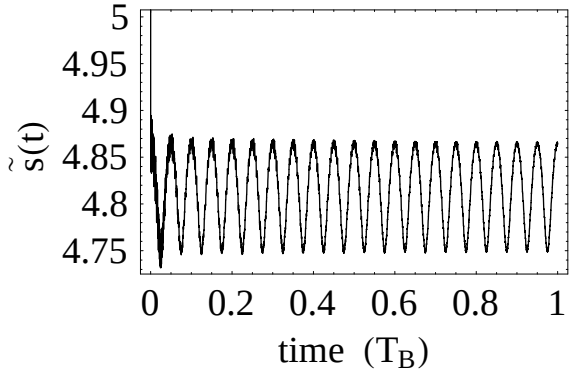

Figure 4.5: Lattice depth as a function of time for $\frac{g_0^2}{\delta\kappa} = 0.5$, $\delta = -3.07 \times 10^9\,\mathrm{Hz}$ and $\eta = 9.8 \times 10^5\,\mathrm{Hz}$. The initial lattice depth is $\tilde{s}(0) = 5.526$.

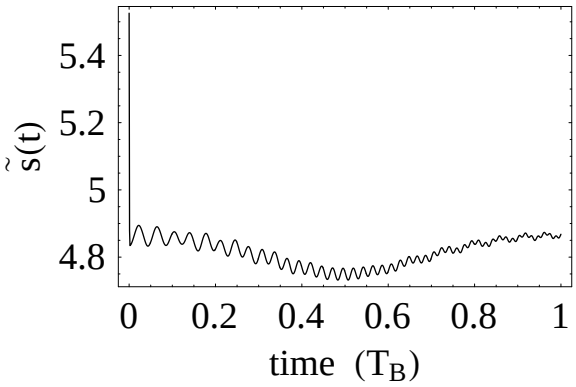

Figure 4.6: Transient (short times) behaviour of the lattice depth for $\frac{g_0^2}{\delta\kappa} = 0.5$. This picture zooms into the first full Bloch oscillation of Figure. 4.5.

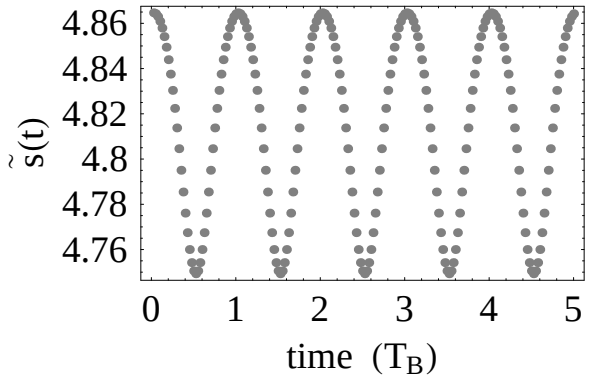

Figure 4.7: Self-consistent solution for the lattice depth for $\frac{g_0^2}{\delta\kappa} = 0.5$, $\delta = -3.07 \times 10^9\,\mathrm{Hz}$ and $\eta = 9.8 \times 10^5\,\mathrm{Hz}$.

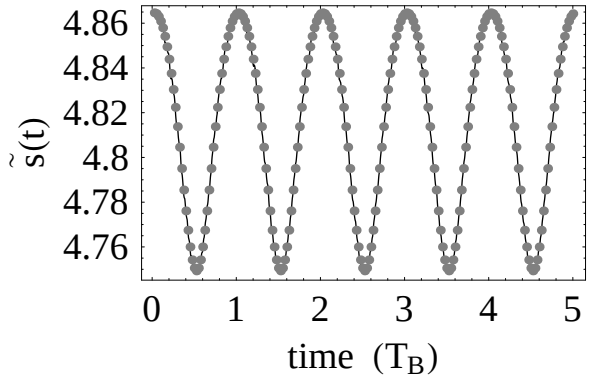

Figure 4.8: Lattice depth as a function of time for $\frac{g_0^2}{\delta\kappa} = 0.5$ compared to the self-consistent solution. The dots represent the self-consistent solution and the continuous line represents the full numerical solution. In this case the parameters are same as in Figure. 4.5 but the initial lattice depth is $\tilde{s}(0) = 4.9$. The full numerical results are in good agreement with the self-consistent solution.

evolution are more pronounced for larger coupling (Fig. 4.6). Let us look at the adiabatic solution for this coupling. Note that once we have chosen an initial wave function and a value for the pump parameter η, the self-consistent solution (Eq. 4.17) is independent of what initial lattice depth you chose. This is evident from Fig. 4.7. On the other hand, as we have already discussed for $g_0^2/(\delta\kappa) = 0.1$, in the full numerical solution of the coupled equations, the initial jump from the atom-less cavity field amplitude to the steady state field amplitude causes transients to appear. The transients are an artefact of our choice of the initial wave function as an eigenstate in the lattice depth $\tilde{s}(0) = 5.526$ whereas we can see from Fig. 4.6 that the lattice depth quickly jumps to a smaller value. We can do away with the transients by starting with an initial wave function that is a Bloch state in the lattice depth obtained from the self-consistent solution at short times. To this end we start our next simulation with all parameters same as above except, the initial lattice depth is given by $\tilde{s}(0) = 4.9$ and the initial wave function is a Bloch function in this lattice with quasi-momentum $q = 0$. This leads to suppression of the transients. We have compared a solution obtained from these modified initial conditions to the self-consistent solution in Fig. 4.8. We see good agreement between the two.

Let us examine the solution plotted in Fig. 4.9 (the case with initial lattice depth $\tilde{s}(0) = 5.526$) in more detail. In the top-most panel we have plotted the lattice depth as a function of time over two BZO. We clearly see that apart from the overall Bloch periodicity there are some fast oscillations. Also, a close examination of the self-consistent solution (Fig. 4.7) or the full solution (Fig. 4.5) will reveal that even the shape of slow oscillations is not perfectly sinusoidal with frequency ω_B. This feature is confirmed from the second panel of the Fig. 4.9 where we have plotted the Fourier transform of the lattice depth (in all our Fourier transform

calculations we subtract out the zero frequency component of the Fourier transform). In this plot we see that not only the Bloch frequency but also its higher harmonics are also present in the spectrum. The self-consistent solution manages to capture this feature which is evident from its agreement with the full numerical solution (Fig. 4.8). This leads to the conclusion that the higher harmonics of the Bloch frequency in the lattice depth spectrum are a manifestation of adiabatic atomic back-action on the light field and may be viewed as a form of amplitude modulation.

In the bottom-most panel of Fig. 4.9 the Fourier transform for higher frequencies is plotted and we see a group of non-harmonic higher frequencies are present. These give rise to the fast oscillations in the lattice depth seen in the top-most panel. Note that these are not present in the self-consistent solution and are hence non-adiabatic in nature. The reason for the appearance of these higher frequencies is that the energy level structure in a periodic system is organized into bands. These higher frequencies are comparable to the Band gaps in the steady state lattice depth. For example in a lattice depth $\tilde{s} = 4.865$, the gap between the ground band and the first excited band varies between $10.5\omega_{\mathrm{B}}$ (between $q = 19/20$ and $q = 21/20$ i.e. the gap at the edge of the band) and $22.9\omega_{\mathrm{B}}$ (between 0 and $q = 2$ i.e. at the centre of the band). This range of frequencies is comparable to the non-harmonic higher frequency peaks we see in the Fourier spectrum of the lattice depth $\tilde{s}(t)$, depicted in the bottom-most panel of Fig. 4.9. Note that in the self-consistent solution we model quasi-momentum dynamics by the Houston wave function and assume all our dynamics is in a single ground band.

Although the higher non-harmonic frequency oscillations are an effect that can be traced back to the fact that we are looking at dynamics in a periodic structure (we try to justify this in the last section of this chapter), the fact that we start with an initial state not quite in the ground band for the lattice depth obtained after the initial transients, enhances this effect. To check this we have plotted the lattice depth as a function of time and the Fourier transform in the Fig. 4.10 for the case where we start with a Bloch function in the initial lattice depth $\tilde{s}(0) = 4.9$. Comparing Fig. 4.9 to Fig. 4.10 we see that the amplitudes of the higher non-harmonic frequencies have been suppressed in the latter.

We continue our analysis by looking at what happens for a larger value of the coupling parameter. We chose $g_0^2/(\delta\kappa) = 1.5$. We chose the initial lattice depth $\tilde{s}(0) = 12.52$ (we have chosen an initial lattice depth larger than what we had chosen for the previous lower coupling values anticipating the fact that transients will lead to a jump from the initial value). This means other parameters have the following values, $\delta = -3.07 \times 10^9$ Hz, initial field amplitude $\alpha_i = 0.2298$ and from $\alpha_i = \eta/\kappa$, we have $\eta = 8.52 \times 10^5$ Hz. As we have discussed before starting with a Bloch state in the lattice depth $\tilde{s}(0) = 12.52$ causes transients. We solve the

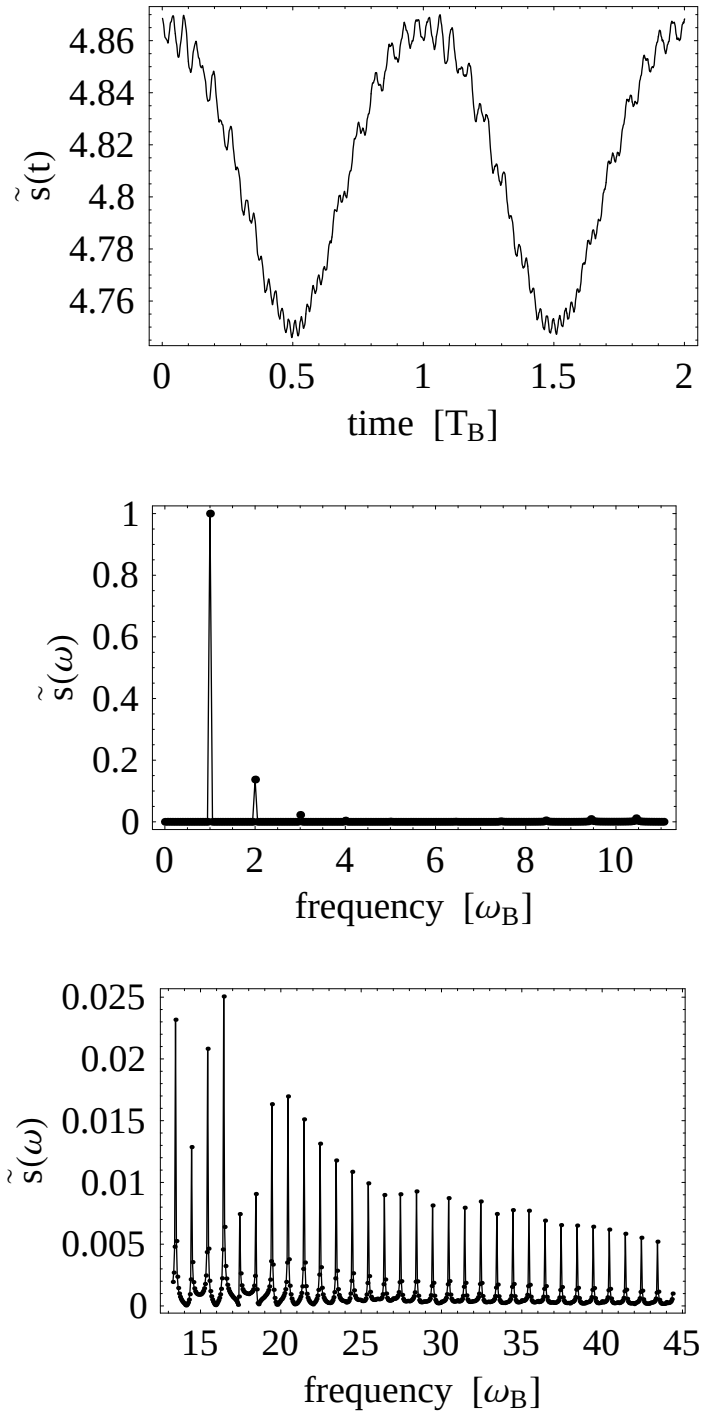

Figure 4.9: In the top-most panel the lattice depth as a function of time is plotted for two Bloch periods for coupling $\frac{g_0^2}{\delta\kappa} = 0.5$, $\delta = -3.07 \times 10^9$ Hz, $\eta = 9.8 \times 10^5$ Hz and $\tilde{s}(0) = 5.526$. In the middle and bottom-most panel the Fourier transform of the lattice depth function has been plotted (amplitudes in the Fourier transform $\tilde{s}(\omega)$ have been scaled by the largest amplitude occuring at $\omega = \omega_B$).

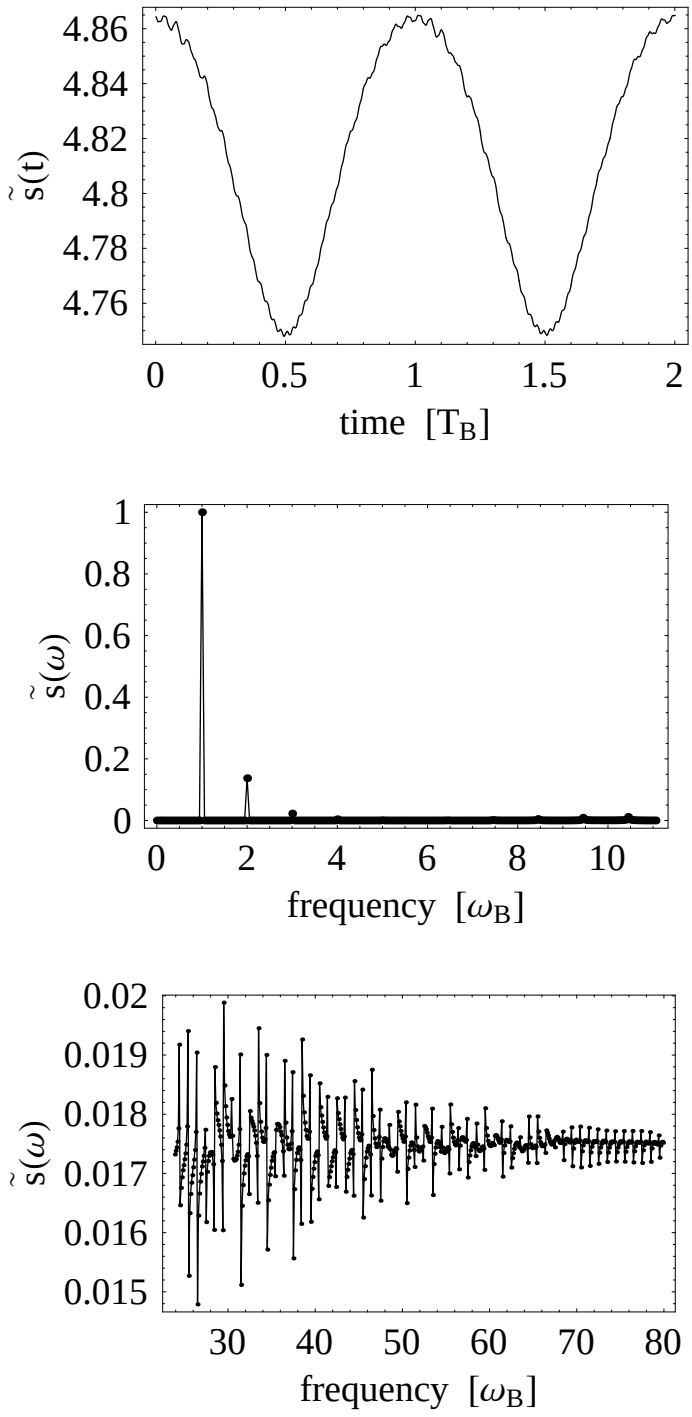

Figure 4.10: In the top-most panel the lattice depth as a function of time is plotted for two Bloch periods for coupling $\frac{g_0^2}{\delta\kappa} = 0.5$, $\delta = -3.07 \times 10^9$ Hz, $\eta = 9.8 \times 10^5$ Hz and $\tilde{s}(0) = 4.9$. In the middle and the bottom-most panel the Fourier transform of the lattice depth function has been plotted (amplitudes in the Fourier transform $\tilde{s}(\omega)$ have been scaled by the largest amplitude occuring at $\omega = \omega_B$). Comparing the above figure to Fig. 4.9, we see that the amplitudes of the non-harmonic higher frequencies have been suppressed in the former due to the choice of initial wave function.

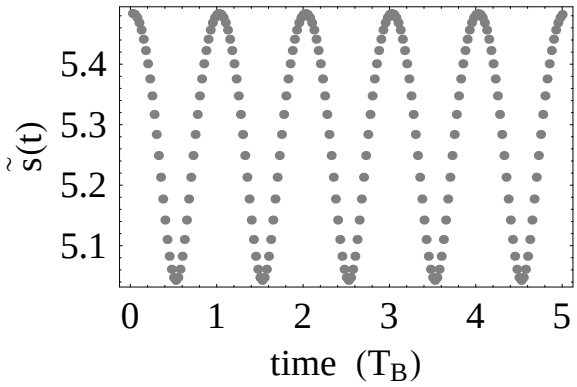

Figure 4.11: Self-consistent solution for the lattice depth for $\frac{g_0^2}{\delta\kappa} = 1.5$, $\delta = -3.07 \times 10^9$ Hz and $\eta = 8.52 \times 10^5$ Hz.

self-consistent problem to determine the choice for our initial conditions. In Fig. 4.11 we have plotted the self-consistent solution and see that at short times the lattice depth takes the value 5.53. We start our simulations with the above parameters but with a Bloch state with quasi-momentum $q_0 = 0$ in a lattice depth $\tilde{s}(0) = 5.53$. The result of this simulation is plotted in Fig. 4.12 and in Fig. 4.13, we have compared the lattice depth calculated in this manner with the self-consistent solution. We see that the calculated value of the lattice depth agrees well with the self-consistent solution. In summary, what we learn

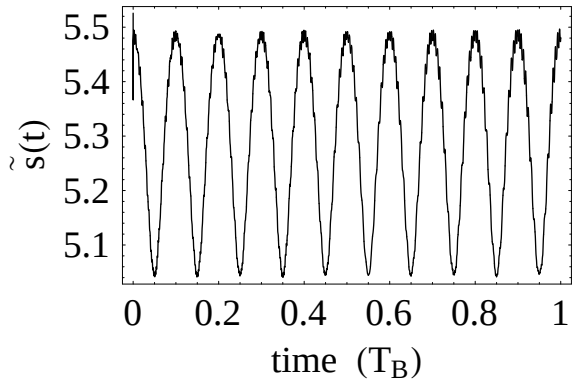

Figure 4.12: Lattice depth as a function of time for $\frac{g_0^2}{\delta\kappa} = 1.5$,$\delta = -3.07 \times 10^9$ Hz and $\eta = 8.52 \times 10^5$ Hz .The initial lattice depth is $\tilde{s}(0) = 5.53$.

from the above numerical results is that despite the intricacies of self-consistent amplitude modulation, the Bloch acceleration theorem carries through and hence the Bloch frequency ω_B is the same as the one in a static lattice. We have verified that the fundamental Bloch frequency is unaffected over a range of values of the coupling parameter $g_0^2/(\delta\kappa)$. We do not present detailed results for other values of $g_0^2/(\delta\kappa)$ but in Fig. 4.14 plot the Bloch frequency as a function of the coupling and see there is very little change in the value of ω_B. Each numerical data point in Fig. 4.14 was obtained in the following manner. A Fourier series

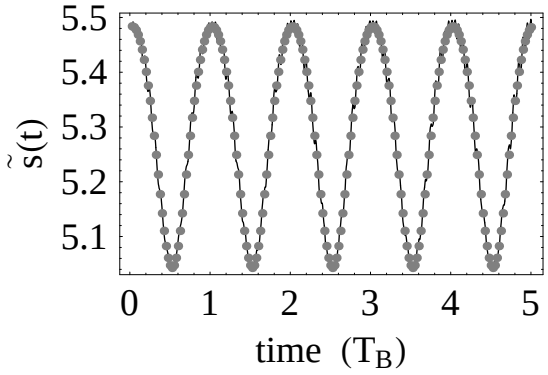

Figure 4.13: Lattice depth as a function of time for $\frac{g_0^2}{\delta\kappa} = 1.5$ (other parameters are the same as Fig. 4.12) compared to the self-consistent solution (represented by the dots on the figure). The numerical and self-consistent solution agree well.

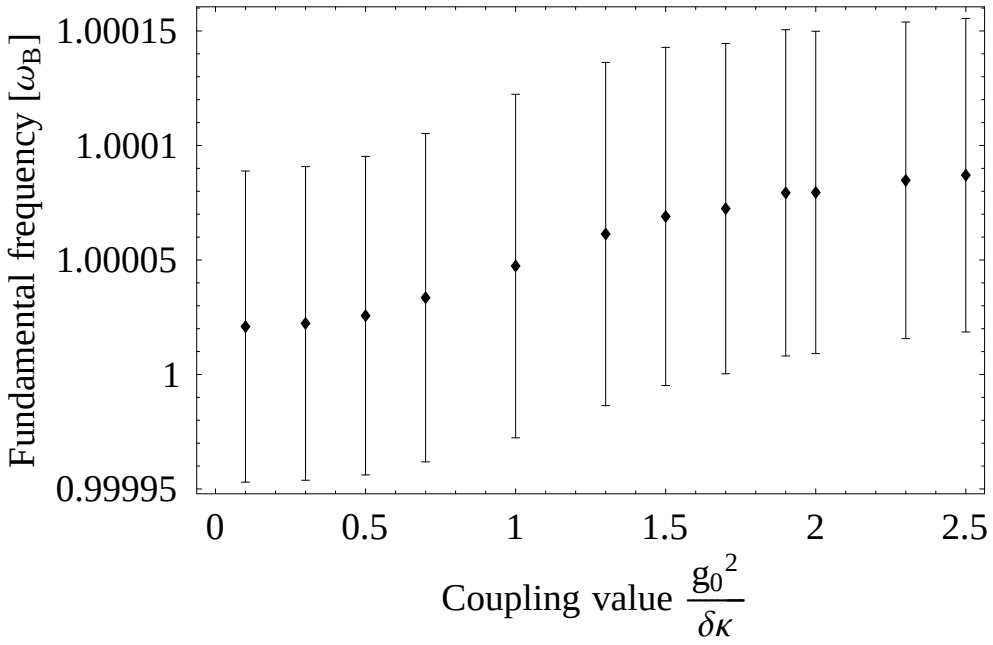

Figure 4.14: Fundamental frequency, in units of ω_{B}, calculated by fitting the lattice depth to a truncated Fourier series is plotted as a function of coupling value. The fundamental frequency of modulation is the Bloch frequency for a range of values of the coupling $g_0^2/(\delta\kappa)$(The trend of increasing best fit values of ω_B with $g_0^2/(\delta\kappa)$ is due to the truncation of the Fourier series and has no physical meaning).

expansion (truncated at the second harmonic) with fundamental frequency ω was fitted to the lattice depth numerical data using the *Mathematica*® function NonLinearRegress [48]. This function calculates a least squares fit to the numerical data and gives the values of the best fit parameters with a confidence interval. Each numerical data point with its error bars gives the range of the best fit value for the frequency ω. The error bars become negligible when you have a numerical data set that perfectly fits the form of the fitting function used. In our numerical data sets, apart from the first and second harmonics of the Bloch frequency we have higher harmonics and non-harmonic higher frequencies as one can see from the Fourier analysis in Fig. 4.9. Hence, we have significant error bars. In spite of this the fitting exercise shows that for a range of values of $g_0^2/(\delta\kappa)$ we have the fundamental frequency of modulation as the Bloch frequency lending robustness to our scheme.

4.5 Non-Harmonic Higher Frequency Oscillations

In this section we will try to justify a statement we made regarding the non-harmonic high frequency oscillations that were seen in the lattice depth calculations discussed in the last section (in this section we use the term higher frequency oscillations to mean only the non-harmonic frequencies and not the harmonics of the Bloch frequency which are adequately explained by the self-consistent solution) . We stated that these higher frequency oscillations have their origin in the fact that we are considering dynamics in a periodic potential. The energy dispersion in a periodic potential is arranged into bands and the presence of higher bands manifests itself as the non-harmonic higher frequency oscillations in observables. To strengthen this argument and to examine the nature of these higher frequency oscillations in some more detail, in this section we consider an atom in a stationary lattice (i.e. no amplitude modulation) and moving under the influence of gravitational force. In the last section we saw that the coupling integral, which is essentially the expectation value of the potential energy of the atom $\langle\cos^2(x)\rangle$, was the quantity that decided the self-consistent lattice depth. In this section we will examine the time dependence of this observable in a stationary lattice. The hamiltonian we consider is $H = \frac{\hat{p}^2}{2M} + \tilde{s}\cos^2 x + Fx$. Let us call the observable under consideration :

$$C_2(t) = \frac{g^2(t)}{g_0^2} = \langle\cos^2(x)\rangle(t) \ . \tag{4.21}$$

We will look at the effect of changing the lattice depth and the force term on $C_2(t)$. We first state a summary of the results, followed by a more detailed discussion and some comments on the physical reasons for the behaviour we see. In all the numerical simulations we start with an atom in a given stationary lattice with an additional constant force. The initial

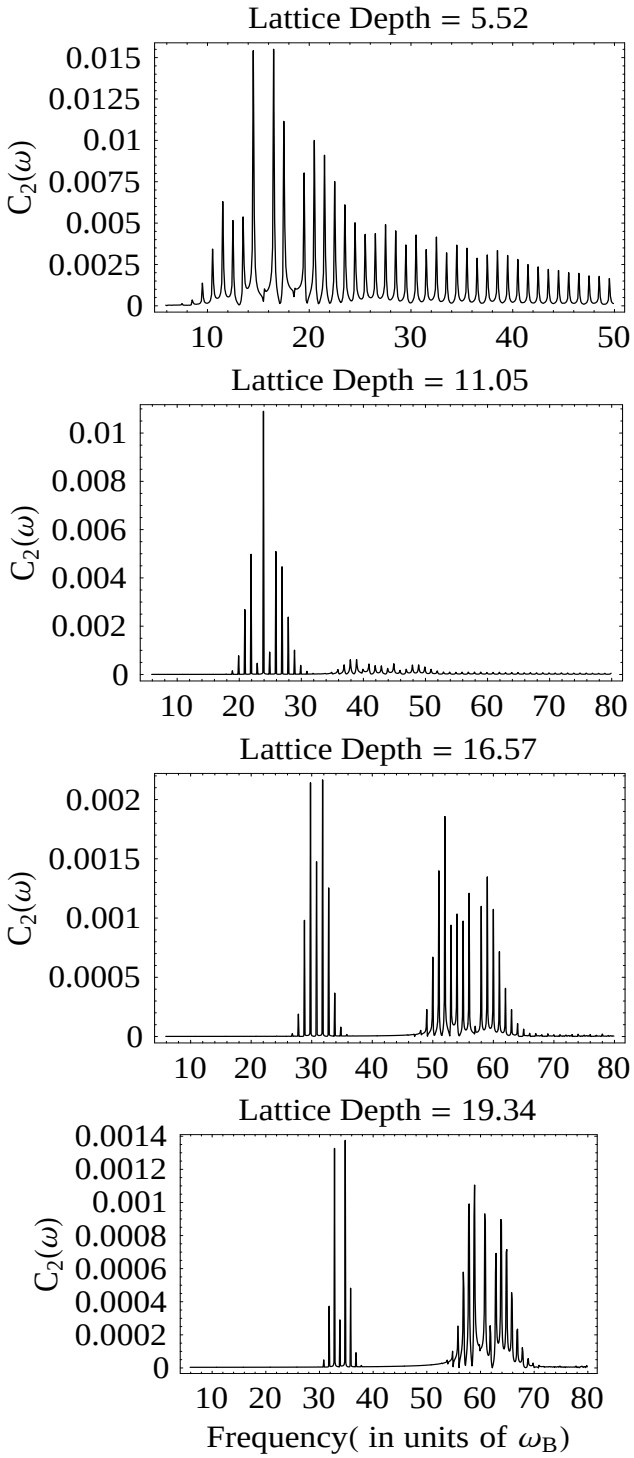

Figure 4.15: Fourier transform spectrum of $C_2(t)$ for different lattice depth values. We see that the higher non-harmonic frequencies observed increase as the lattice depths increases in agreement with the fact that in a deeper lattice the band-gaps are larger.

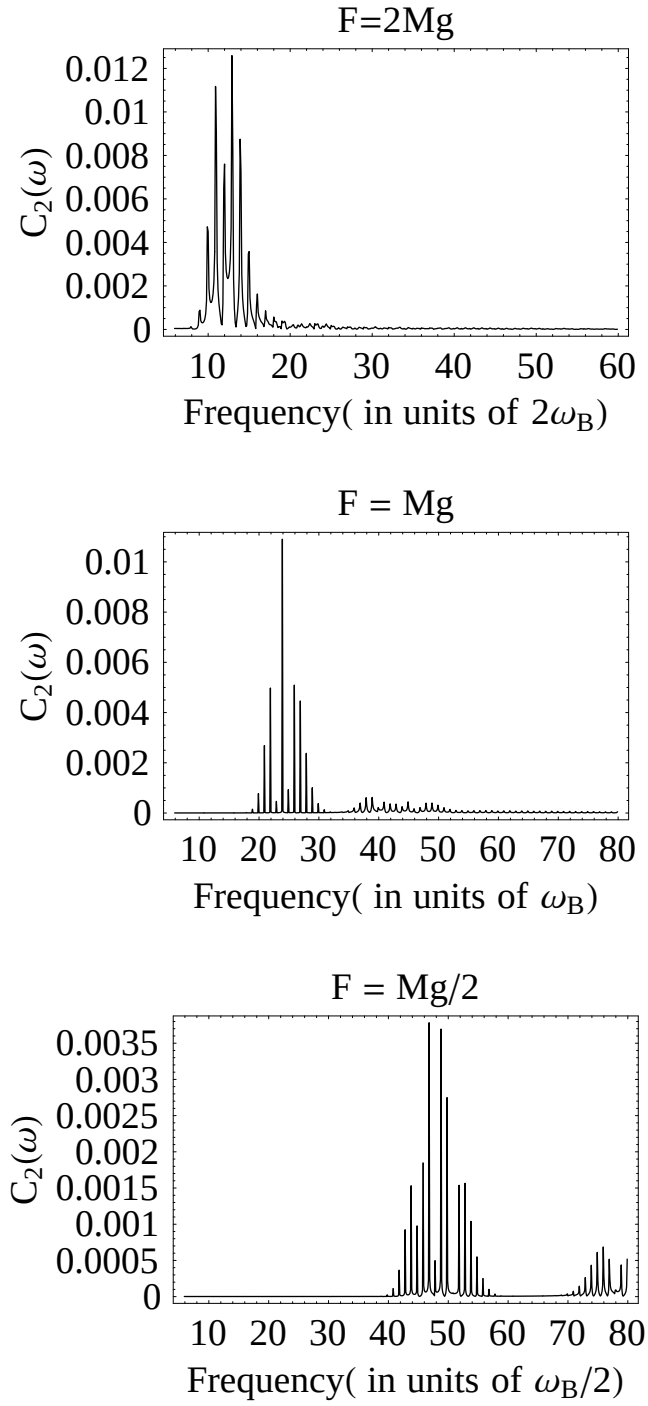

Figure 4.16: Fourier transform spectrum of $C_2(t)$ for different values of F and lattice depth = 11.05. The force term decreases as we go from the top-most panel downwards. Although the scale of the frequency axis changes for the different panels, we see that the absolute value of the peak frequency (take to be the frequency value with largest Fourier amplitude) stays the same.

wave function of the atom is assumed to be a Bloch function with quasimomentum $q = 0$. The main results are as follows :

- The observable $C_2(t)$ is modulated mainly at the Bloch frequency but there are higher frequency oscillations at frequencies that are not harmonics of the Bloch frequency.
- At a given force value, when we increase the depth of the lattice we see that the higher frequencies shift to larger values and their amplitudes become smaller.
- At a given value of lattice depth as we increase the force term we see that the value of the higher frequencies remain the same but the amplitude of the higher frequencies increases.

Let us now describe the simulations in detail. The linear applied force we use is $F = Mg$, the Bloch frequency is given by $\omega_{\mathrm{B}} = Mgd/\hbar$. In the first set of numerical solutions, we changed the potential depth with a fixed F. The observable $C_2(t)$ was calculated over 10 Bloch oscillations and Fourier transformed. In all our Fourier transform calculations we subtract out the zero frequency component of the Fourier transform. Looking at Fig. 4.15 we see that as we increase the lattice depth, the value of the non-harmonic higher frequencies increases. This agrees with our expectation that the excitations are due to higher band effects since in deeper lattices the band gaps are larger. The amplitude of the non-harmonic higher frequencies of the Fourier transform, which is related to the net change in $C_2(t)$ over one oscillation, decreases for deeper lattices. This is because for deep lattices the band dispersion becomes flat and the net change in observables, as the quasi-momentum evolves in the band, is small. Another way to state this fact is to appeal to the tight binding limit which is the right description for very deep lattices. In this approach the periodic part of the Bloch function (writing Bloch functions as $\phi_k(x) = e^{ikx}U_k(x)$), $U_k(x)$ does not change as the quasi-momentum evolves within a band. This means expectation values, like the one we are considering, remain constant in time.

Next we consider Fig. 4.16 where the Fourier transform of $C_2(t)$ for a given lattice depth ($\tilde{s} = 11.05$) and three different values of the applied force F has been plotted. The Bloch frequency changes from top panel to the bottom panel as follows, $2\omega_{\mathrm{B}}$, ω_{B} and $\omega_{\mathrm{B}}/2$. The figures show that the frequency at the peak is unchanged. The value of frequency for which the Fourier amplitude is largest is picked as the frequency at the peak. In the first figure it occurs at the frequency $12.9 \times 2\omega_{\mathrm{B}}$, in the second it occurs at $23.9 \times \omega_{\mathrm{B}}$ and in the third it occurs at $46.8 \times \omega_{\mathrm{B}}/2$. The frequency at the peak for the three different values of force namely $F = Mg/2$, $F = Mg$ and $F = 2Mg$ do not share the exact expected relation of 1/2:1:2. This can possibly be due to the fact that there are a bunch of closely spaced peaks in Fig. 4.16 and the way we picked the frequency at the peak was simplistic.

The force term F is decreasing from the top to the bottom panel and we see that the amplitude of the high frequency oscillations also go down but their frequency remains the same.

The next step is to compare our results with previous studies of BZO that observed such non-harmonic higher frequencies. Since the two references we discuss, A.M. Bouchard and M. Luban [50] and P. Abumov and D.W.L. Sprung [51], consider BZO in semiconductor superlattices let us introduce a few terms that are used in them. The net drop in potential energy due to the force term per one lattice period is known as the bias, which has the value $F\lambda_c$. Another parameter that plays an important role is the band width of the lowest band, call it Δ_{W}. This is important because the band width is the length in energy space covered by the quasi-momentum during a BZO. In a tight-binding lattice model the energy dispersion is modelled by $E(k) = -\frac{\Delta_{\mathrm{W}}}{2}\cos(k_c d)$. The next important parameter is the band-gap Δ_{E}. For our analysis we consider only the band-gap between the lowest band and the first excited band. Finally we can model the individual lattice sites (at the bottom of the wells) as a harmonic oscillator and the effective harmonic frequency at the bottom of the wells is given by $\omega_{\mathrm{ho}} = 2\frac{E_R\sqrt{\tilde{s}}}{\hbar}$, where $E_R = \hbar^2 k_c^2/(2M)$ is the atomic recoil energy. In Table. 4.1 we compare the peak of the higher frequency oscillations observed in Fig. 4.15 for different lattice depths with the band-gap frequency and harmonic frequency. These frequencies are comparable lending credibility to our earlier arguments that we are observing higher band effects.

The energy structure of a lattice is responsible for two slightly different phenomenon, each of which can give rise to high frequency oscillations. The first effect is Zener tunneling. This describes the tunneling probability of the atom between bands (originally discussed by [1]) and the probability of such a tunneling event between bands seperated by Δ_{E} is given by :

$$\gamma = \exp(-\frac{m\lambda_c^2}{4\hbar^2}\frac{\Delta_{\mathrm{E}}^2}{F\lambda_c}) \ . \tag{4.22}$$

This phenomenon is significant when the ratio $F\lambda_c/\Delta_{\mathrm{E}}$ is large. This is definitely not the regime we are in, as is evident by looking at Table 4.2. It is also interesting and obvious to note that the ratio $F\lambda_c/\Delta_{\mathrm{E}}$ is nothing but the inverse of the bandgap frequency in units of Bloch frequency, which as we already noted is comparable to the high frequencies in $C_2(\omega)$ spectrum.

The other phenomenon that can give rise to higher frequency oscillations, discussed by [50] and [51], are the intrawell oscillations. This is basically sloshing around of the wave function inside the individual wells of the lattice [50]. Ref [50] states that the regime for which intrawell oscillations become important are when the ratio of bias $F\lambda_c$ to the band

Table 4.1: Comparison of non-harmonic higher frequency peaks observed in Fig. 4.15 with other relelvant frequencies namely the band-gap between the ground and first excited band Δ_{E} and the harmonic frequency ω_{ho}.

LatticeDepth	Peak(from $C_2(\omega)$)	$\Delta_{\mathrm{E}}/\hbar$	ω_{ho}
5.52	16.5	15.51	20.8
11.05	23.9	23.87	29.47
16.57	31.8	30.77	36.1
19.34	34.8	33.77	38.9

width Δ_{W} is large but the ratio of bias to band gap Δ_{E} is still small i.e. away from the Zener tunelling regime. Again looking at Table. 4.2, we are in such a regime and the validity of this regime increases as we increase the potential depth. This is because the dynamics in each well of the lattice becomes independent, for deep lattices.

Table 4.2: Correlation between bias to bandwidth ratio ($F\lambda_c/\Delta_{\mathrm{W}}$), bias to band-gap ratio ($F\lambda_c/\Delta_{\mathrm{E}}$) and non-harmonic higher frequency values at the peak ((the frequency value with the largest Fourier amplitude)) and their amplitude.

Lattice Depth	Peak Frequency	Peak Amplitude	$\frac{(F\lambda_c)}{\Delta_{\mathrm{W}}}$	$\frac{(F\lambda_c)}{\Delta_{\mathrm{E}}}$
5.52	16.5	0.015	0.98	0.06
11.05	23.9	0.011	3.73	0.041
16.57	31.8	0.002	11.84	0.032
19.34	34.8	0.0014	20.04	0.029

Ref [50] model intrawell oscillations by considering individual wells as finite length constant potential boxes with infinite potential energy boundaries. They start with a superposition of Wannier wave functions (which are onsite localised wave functions got by Fourier transforming the Bloch functions) in the ground and first band. They look at the $\langle x \rangle$ for such a wave function and see oscillations in this observable at the frequency $\frac{E_1 - E_0}{\hbar}$ where the energies are the energy levels in a box. They also add that using E_1 and E_0 as the average band energies of the bare lattice also gives them the right intrawell oscillation frequency. In comparison we start with a Bloch state in the lowest band (which is a linear combination of Wannier states from different wells). We calculate $< \cos^2(x) >$ and observe high frequency oscillations with frequency values close to the band-gap frequencies. Thus it seems likely that we are also observing an effect due to intrawell oscillations. The observable $C_2(t) = g^2(t)/g_0^2$ goes into determining the steady state solution (Eq. 4.13) for the lattice depth in the amplitude modulated BZO case. We emphasize again that in the Fourier spectrum of the lattice depth as a function of time (Fig. 4.9) we observe two features. There are higher harmonics of the Bloch frequency that are well explained by using the adiabatic self-consistent amplitude modulation described in Eq. 4.17 which takes the atomic back action on the field into account. Apart from this there are non-harmonic higher frequencies

observed and they are comparable to the band gaps in the energy spectrum. Similar non-adiabatic effects are also observed in the observable $C_2(t)$ for BZO in stationary lattices as discussed above. Hence we conclude that the non-harmonic frequencies are related to the intrawell oscillations phenomena considered for the stationary lattices.

Thus, we see from the numerical solutions that the field amplitude and phase are modulated at the Bloch frequency. The calculated self-consistent solution for the lattice depth captures the main feautures of the full numerical solution namely the modulation at Bloch frequency and the presence of higher harmonics of the same. It fails to explain the higher non-harmonic frequencies which we understand as a phenomenon of intrawell oscillations.

Chapter 5

Experimental Details

5.1 Introduction

In the second section of this chapter we give an overview of the various experiments that have already been proposed to study BZO of cold atoms. The main feautures of the experiments and also the limitations that they face are described. In the third section a rough schematic of the experiment we propose is explained.

5.2 BZO Experiments

In this section we will need some of the definitions used in the earlier chapters for the experimental parameters. k_c denotes the wavenumber of the standing wave field experienced by the atom, $E_R = \hbar^2 k_c^2 / (2M)$ denotes the atomic recoil energy, $\tilde{s}$ denotes the lattice depth in units of E_R and Γ the width of the atomic level.

The general procedure in cold atoms experiments aiming to study BZO consists broadly of the following stages. The first step is to cool atoms from room temperature down to very low temperatures (ranging from microKelvins to nanoKelvins depending on whether one wants to make a BEC or not). A variety of techniques are used to achieve this cooling and details can be found from the references [9, 52, 53]. Once the atoms are cooled down, they are transferred to the optical lattice potential, which is in general created by the interference of two counter-propagating laser beams. The process from here on allows the atoms to evolve in the optical lattice with a constant force, which can either be a naturally occuring inertial force like gravity or a non-inertial force created by chirping the frequencies of the two lasers that create the optical lattice. The optical lattice is then switched off after different holding times in the lattice and the atoms are allowed to ballistically expand. After this they are destructively imaged using a weak resonant probe that casts a shadow of the

atomic distribution, which is captured using a CCD camera. This gives information on the position space atomic distribution at the time of imaging which can be used to map out the initial momentum space distribution. This measurement process is called a time-of-flight measurement.

The first experiment to observe BZO in cold atoms was reported by M. Ben-Dahan *et al.*, in [5]. Some of the points made in this work are very relevant to our proposal too. The group used ultracold cesium atoms, with atomic transition wavelength $\lambda_0 = 852\,\text{nm}$ and width $\Gamma = 2\pi \times 5.3\,\text{MHz}$. The lattice frequency was detuned from the atomic frequency by $\delta = 2\pi \times 30\,\text{GHz}$. The depth of the lattice was varied between $0 < \tilde{s} < 6$ with the recoil energy $E_R = h \cdot 2.068\,\text{kHz}$. Since most of these experiments were in the far-detuned limit, spontaneous scattering of photons was very small. Neverthless, a single spontaneous emission event could impart a momentum recoil as large as the Brillouin zone momentum (given by $2\hbar k_c$) of the lattice and hence affect Bloch dynamics. Thus, it becomes imperative to compare the spontaneous emission rate to the time scales over which BZO are measured. In their case the scattering rate $\Gamma_{sc} \approx 4\,\text{s}^{-1}$, which can be totally neglected for their observation time scale that is of the order of 1 ms. They mimiced a constant external force by introducing a tunable frequency difference $\delta\nu(t)$ between the counter-propagating lattice beams. The reference frame in which the optical potential is stationary moves with a velocity of $\delta\nu(t)\lambda_c/2$ and for a linear variation in time of $\delta\nu(t)$ a constant inertial force $F = -ma = -m\lambda_c \frac{d}{dt}\delta\nu(t)/2$ is exerted on the atoms. The ranges of acceleration considered in the experiment are $0.43\,\text{ms}^{-2} < a < 12.2\,\text{ms}^{-2}$.

One important observation that they make concerns the loading of the cooled atoms into the optical lattice. Since they wanted the atoms to occupy the ground state of the lattice, they have to switch on the lattice potential adiabatically and prevent transitions to higher bands in the process. This is also relevant to our case, where we should make sure that the switching on of the single-mode field inside the cavity does not cause excitations to a higher band (although in an alternate scenario we can imagine cooling the atom inside the cavity [54]). Another relevant point in the experiment was the choice of the initial state for the atoms in the lattice. In our theoretical analysis of the problem in the previous chapters we assume we always start with a single Bloch wave with a well defined quasi-momentum q (a picture of a Bloch wave with $q = 0$ in momentum space is shown in Fig. 5.2). In an actual experiment one starts with a narrow distribution in quasi-momentum space (look at Fig. 5.3) and the central quasi-momentum evolves according to the Bloch acceleration theorem (Eq. 3.17). In Fig. 5.1 we plot the Bloch evolution of an initial Gaussian state in quasi-momentum space centred at $q = 0$ and standard deviation $k_c/9$. In the experiment [5] they started with a Bloch state around q=0 and width given by $k_c/18$ which is much

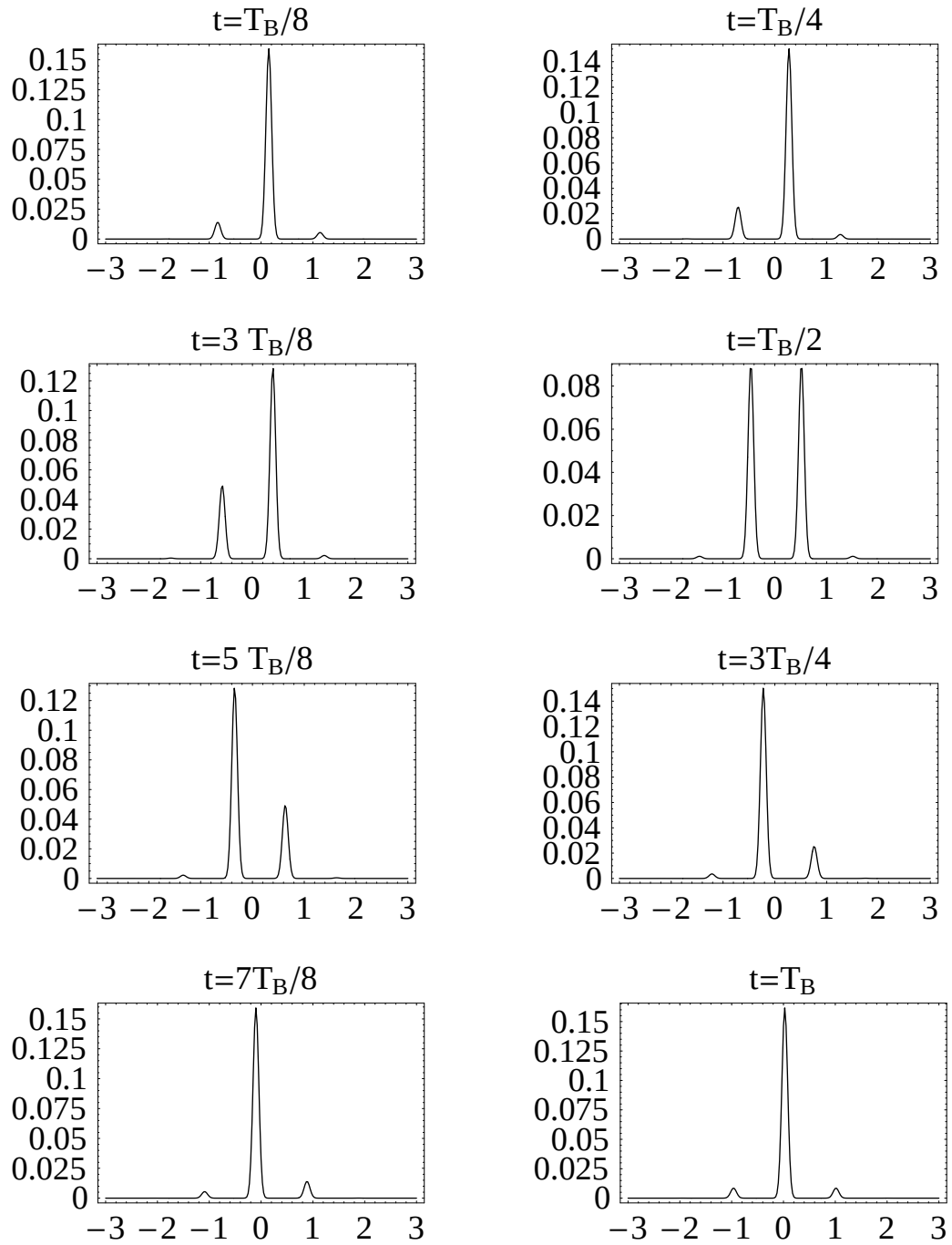

Figure 5.1: Time evolution in momentum space of a wave packet with a narrow distribution in quasi-momentum space. Bragg reflection occurs at $t = T_B/2$

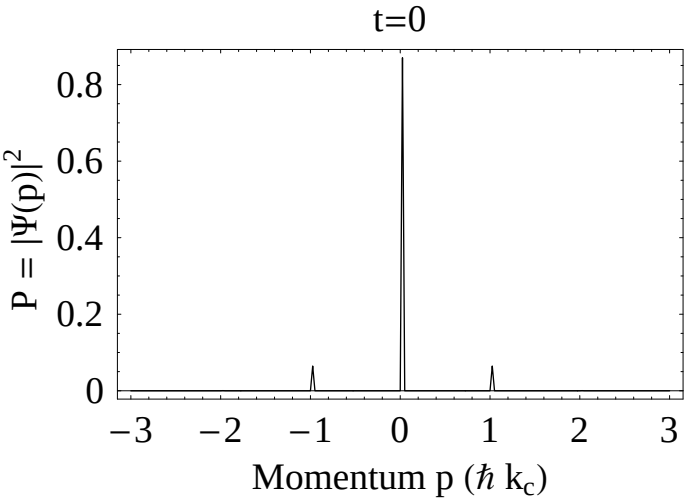

Figure 5.2: Momentum space distribution of a Bloch function for a lattice depth $\tilde{s} = 4$ and q=0.

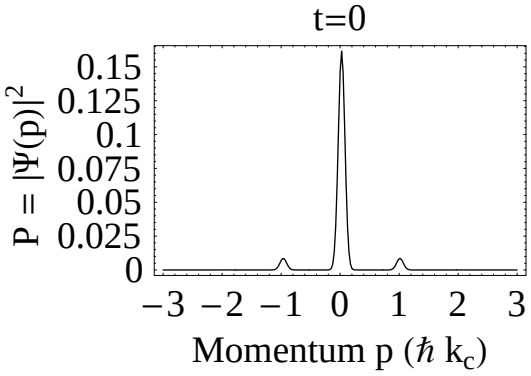

Figure 5.3: Momentum space distribution for a gaussian distribution in quasi-momentum space around q=0 for a lattice depth $\tilde{s} = 4$.

less than the width of a Brillouin zone ($2k_c$). Theoretical analysis of the experiment was carried out by dividing the initial momentum distribution into channels centered around different quasi-momentum. Bloch evolution was assumed for each of the channels and the contributions of different channels were combined to obtain the mean atomic velocity. This method agreed well with their experiment. This means that our theoretical study carried by using a single Bloch wave initial state can be extended in the same manner to explain results from the proposed experiment.

The next experiment we consider is the one by Anderson and Kasevich [6]. In this experiment a BEC ^{87} of Rb atoms (transition wavelength $\lambda_0 = 780\,\text{nm}$) was used in a vertically oriented optical lattice (wavelength of light $\lambda_c = 850\,\text{nm}$ i.e. detuning $\delta \approx 2\pi \times 31.7\,\text{GHz}$). The Zener tunneling probability of atoms in a lattice is maximum when the momentum is close to the band edges. During a BZO the atomic momentum periodically

approaches the band edges and hence one gets increased tunneling periodically. In this experiment shallow lattices ($\tilde{s} = 1.4$) were used to enhance Zener tunneling. They observed pulses of atoms, by destructively imaging them, leaving the vertical lattice periodically after Zener tunneling (at the Bloch period). This helped them to measure T_B and hence the value of acceleration due to gravity. The maximum holding time in the lattice they consider, was of the order of 50 ms which was much less than the time scale at which off-resonant spontaneous scattering is important.

In [24], Morsch *et al.*, used ^{87}Rb condensate atoms in an optical lattice. After a finite amount of interaction time the lattice was switched off and the atoms were destructively imaged. Repeating this process for different amounts of interaction time they mapped the expectation of atomic velocity as a function of time and saw that it had an oscillatory structure at the Bloch period T_B. One important feature required for the observation of BZO in cold atom systems is a sufficiently narrow distribution in quasi-momentum space which will result in a well resolved peak structure in momentum space. Interatomic interaction in BECs quickly broadens the distribution in real momentum space, as opposed to quasi-momentum space (if interactions are significant, the initial momentum space distribution will also be broad). This makes it difficult to observe more than a few oscillations. The experiment of Morsch *et al.* aimed to address this issue by trying to verify the claim that the effect of interactions is to modify the lattice depth seen by the atoms [55]. They accelerated the lattice by chirping the standing wave lattice lasers. The spontaneous scattering rate of $10\,\mathrm{s}^{-1}$ was insignificant since the interaction times of the atoms and the lattice was of the order of milliseconds. The lattice depth they used was $\tilde{s} = 11.04$ (the atomic level and laser light were detuned by $28 - 35$ GHz) and the acceleration values they used is $0.94\,\mathrm{ms}^{-2}$. Apart from this they also used shallow lattices to observe Zener tunneling and used that to estimate the effective potential due to the interactions in a BEC.

The next experiment we discuss is by G. Roati *et al.* [25]. There are two main limitations of observing BZO by a momentum space study of BEC atoms. The first one is the fact that interactions broaden the distribution and lead to loss of contrast. The second related problem is that using deeper lattice depths to prevent Zener tunneling increases atomic density in the condensate, leading to enhanced interaction. In this experiment this problem was avoided by using ultracold Fermions where the Pauli principle suppresses collisional interaction at low temperatures. They used ultracold ^{40}K atoms sympathetically cooled (close to the Fermi temperature T_F) using ^{87}Rb atoms. The atomic transition line used was $\lambda_0 = 873$ nm and the lattice depths ranged from 1-4 E_R and the constant force was gravity. The initial state of the ultracold atoms had a width of $0.75k_c$ and was in the lowest band of the lattice. They provide an interferometric interpretation to the observation of BZO. The

eigenstates of a combined periodic and gravitational potential are the Wannier-Stark (WS) states [56]. The defining feature of WS states are their ladder energy structure separated by $\tilde{\Delta}_E = Mg\lambda_c/2$. The initial state in their experiments was closer to a Bloch state and hence can be thought of as a coherent superposition of different WS states. Because of the energy difference, neighbouring states evolved in time with phase difference $\Delta\phi = \tilde{\Delta}Et/\hbar$ and their interference pattern was periodic in time with period $T_B = h/\Delta E$. They studied the momentum distribution of the atoms by the time-of-flight techniques described earlier and tracked the peak position of the momentum distribution for about 110 Bloch periods. This is significantly more than the number of oscillations seen for BECs and they showed that the momentum distribution of BEC atoms broadens more quickly than the distribution for the Fermi atoms. They discuss the application of such a measurement to measuring gravitational forces with high spatial resolution. The spatial extent of the atoms in the lattice depends upon the width of the Wannier-Stark state which goes as Δ_{W}/F, wher Δ_{W} is the band width and F is the force. They note that in a tighter lattice the vertical extent of the atom can be made small since Δ_{W} is smaller. One important observation they made was that, although having a tighter lattice suppresses Zener tunneling and/or confines the atoms, it can have an unwanted effect that any intensity gradient along the axis of the optical lattice will produce extra forces that will hamper a precision measurement. Other sources that contribute to broadening the momentum space spectrum include intensity and phase noise in the laser beams.(Collisional loss sources due to p-wave collisions in Fermions have a characteristic time of 100 s for their samples making it insignificant on the interaction time scales considerered.)

The next experiment we discuss is the one by G. Ferrari *et al.*, [28]. Their aim (to measure gravity at the micrometer scale) is very close to our aim and the experimental setup for our proposal will share some similarities. They used ultracold ^{88}Sr atoms (transition wavelength $\lambda_0 = 461\,\mathrm{nm}$) in a vertically aligned optical lattice (so the force is gravity) with lattice wavelength ($\lambda_c = 522\,\mathrm{nm}$). The optical lattice was created by using a single laser retro-reflected by a mirror. We note that this is similar to the way a single mode is created in an optical cavity. In a precision measurement using ultracold atoms, one source of noise/broadening is the interaction of the atoms with stray electromagnetic fields. ^{88}Sr atoms have zero orbital angular momentum and nuclear spin in their ground state, which means they are less affected by stray electromagnetic fields. They also have remarkably small atom-atom interactions meant that collisional broadening is minimal. They make an interesting point on the choice of lattice depths. Their argument against very large lattice depths (high intensity beams), is that this will reduce the amplitude of oscillation of the mean momentum, making it difficult to measure BZO. On the other hand an increased

intensity will mean larger confinement in the radial directions preventing loss of atoms and hence a depth of $\tilde{s} = 10$ was chosen balancing the two effects. Thousands of BZO up to a total time of 12 s, using time-of-flight measurements and absorptive imaging techniques described earlier, are observed. The imaging data was used to calculate the peak momentum and the width of the momentum distribution as a function of time. From the data the Bloch period was calculated as $T_B = 574.568$Hz, which gave the value of acceleration due to gravity as $g = 9.80012(5)\text{ms}^{-2}$ (sensitivity of $5 \times 10^{-6} g$). Another source of decoherence, which was relevant to their setup, was the vibrations of the retro-reflecting mirror. It is observed that the collisions of the ultracold atoms with the hotter background vapor pressure inside the cooling MOT trap reduces the signal to noise ratio but does not affect the coherence of the atomic distribution. For the sake of comparison we note that the absolute gravimeter measurements on the website of NGS Geosciences Research Division, USA [57] claim an accuracy of 1 part per billion of g or more precisely $1.1 \times 10^{-8} g$.

In the concluding part they talk about using this setup to measure deviations from Newton's law. The idea of investigating short range gravity with atomic probes was discussed first by [58] and later by [23] and preliminarily demonstrated by [59]. Deviations from Newtonian law can be described by using a phenomenological potential to describe gravity [23] :

$$V(r) = -G\frac{m_1 m_2}{r}\left(1 + \beta e^{-r/\lambda}\right) \ , \tag{5.1}$$

where β gives the strength of the deviation from Newton's law and λ gives the spatial range of the deviation. Recent results using microcantilever detectors [62] (discussed in more detail at the end of the section) lead to extrapolated upper limits of $\beta \approx 10^4$ for $\lambda \approx 10\,\mu$m, but for distances below $10\,\mu$m direct measurements have not been performed. Ref. [28] propose to use a thin sheet of a high density material as the source producing the gravitational field that the atomic cloud moves in. This source can be placed very close to the atoms. The small size and high sensitivity of the atomic probe allows it to access shorter ranges without the need to extrapolate as in the case of macroscopic probes. A material of density ρ and thickness t_0, gives Newtonian gravitational acceleration of $a = 2\pi G\rho t_0$. For $t_0 \sim 10\,\mu$m and $\rho \sim 20$ g/cc (e.g. gold or tungsten), the resulting acceleration is $a \sim 10^{-10}\,\text{ms}^{-21}$. Thus, measuring the Bloch frequency at $10\,\mu$m will provide a check on the extrapolated values of β and λ obtained from cantilever experiments. Non-gravitational effects (surface forces like van der Waals and Casimir forces) can be reduced by using conductive screens and also repeating experiments with different source masses. Using isotopes of Sr having different masses will again distinguish gravity from the other surface forces.

[1] Deviations from this Newtonian acceleration can take large values as we will see later from the discussion of cantilever experiments and hence can be detected independent of the very small Newtonian force

Another interesting proposal by I. Carusutto *et al.*, in [29], concerns the measurement of the Casimir-Polder(CP) force near a dielectric surface. They consider the use of spin polarized cold Fermi atoms in a vertical optical lattice. The idea is to use the deviation of the Bloch frequency, from its value in Earth's gravitational field, due to the presence of the CP force near the surface. They want to measure the CP force with very high spatial resolution. Hence, the real space amplitude of the BZO is required to be small. This amplitude has an order of magnitude Δ_W/F where $2\Delta_W$ is the band width and F is the constant force. The presence of a larger force like gravity reduces this amplitude and increases the spatial resolution and makes it easy to detect the deviations which contain the value of the CP force. This proposal serves to illustrate the variety of measurements that can be performed with a simple central idea, that of BZO.

We end this section with a description of macroscopic experiments that aim to probe gravity at short ranges (a good review of the subject is available in [60]). The general idea in such experiments is to measure the gravitational interaction between two test masses (macroscopic objects that have small dimensions) at very short distances. One of the masses, called the detector, is usually a cantilever and other test mass is called the driving mass, since it is driven at a frequency close to the resonance frequency of the detector mass. The gravitational interaction between the masses, modelled as in Eq. 5.1, is expected to show up as a resonant signal from the test mass motion.

To be more specific we consider two recent experiments in this area. The first experiment we consider was done by the group of John Price at Colorado [61]. In their experiment the test masses were planar in geometry which helped to concentrate most of the mass density at the length scale of interest. As they note, the flat plates are nominally a null geometry with respect to $1/r^2$ forces, which is important for suppressing Newtonian forces relative to short-range effects. The source mass consists of a 35 mm $\times$ 7 mm $\times$ 0.305 mm node-mounted tungsten reed. This source mass was driven at its second cantilever mode, whose frequency was matched to the resonance frequency of the detector mass using a piezoelectric transducer (a device that converts an electrical input into a mechanical output). The detector mass was a 0.195 mm thick tungsten torsional oscillator. A stiff conducting shield suspended between the test masses suppresses electrostatic and acoustic backgrounds. The shield limited the minimum separation between test masses to 100 microns. With the help of some standard techniques, like the use of vacuum bell jars, background noise due to acoustic, electromagnetic sources were suppressed. The only limiting factor in the end is the thermal noise due to finite temperature (305 K in their case). The motion of the detector mass was converted to a electric signal using a capacitive transducer. In their data the signal observed agreed well with predictions from thermal noise and no deviation larger than the

thermal noise was detected after 22 hours of integration time (as they observe in [60], this corresponds to a force sensitivity of about 10^{-15} N). To set limits on the parameters β for different λ in Eq. 5.1, they equated the deviation expected due to resonance interaction as a result of the Yukawa type force to the thermal noise observed. Apart from this, to take the precise geometry and the systematic error into account, the non-Newtonian Yukawa type force between the test masses was computed numerically and constraints on β was calculated using a maximum likelihood technique. From their methods they have obtained a limit of $\beta \leq 10$ for $\lambda \sim 100\,\mu$m and $\beta \leq 10^8$ for $\lambda \sim 10\,\mu$m.

The second experiment we discuss was carried out by the group of A. Kapitulnik at Stanford [62]. The idea in this experiment was, as in the previous experiment, to measure short range gravitational forces between masses with sizes comparable to the separation desired. The detector mass in this experiment was a gold prism ($50 \times 50 \times 30\,\mu$m^3) placed on a silicon cantilever ($5\,\mu$m wide). The drive mass, comprised of a gold meander pattern embedded in a silicon substrate creating an alternating pattern of gold and silicon bars, was mounted on a piezoelectric bimorph at a vertical distance of $25\,\mu$m. The value of the vertical separation was limited in part by the presence of a stiff silicon nitride shield to reduce electromagnetic fields between the masses. The driving mass was oscillated along the horizontal direction, while the vertical separation was maintained, using the piezoelectric morph at a subharmonic of the resonant frequency of the test mass cantilever. The differing mass densities of gold and silicon bars on the driving mass sets up an alternating gravitational field at the detector mass. The motion of the cantilever on resonance was measured using a fiber interferometer and the force between the masses was deduced from this. Thermal noise provided a limit on the measurements of cantilever motion. This was reduced by using cantilevers with small spring constants and high quality factors in vacuum. In a cryogenic set up with temperatures around 10 K the thermal noise limit was approximately $2.5 \times 10^{-16}\,\mathrm{N}/\sqrt{\mathrm{Hz}}$. The separation of the signal frequency from the drive frequency, the shield between the masses, and the use of non-magnetic test masses for the measurement reduced the effect of other possible backgrounds. The geometry of the driving mass, with alternating gold and silicon bars, provided an important degree of freedom that helped to distinguish between true gravitational coupling and other backgrounds. The force on the detector bar was measured for different mean horizontal positions of the driving mass. Since the gold and silicon bars each had a length of $100\,\mu$m, the force at the detector mass was expected to be a periodic function of the mean horizontal position. The data collected for the force had this apparent periodicity and was slightly larger than the approximate level of thermal noise. The numerical data for the force was fitted to a Yukawa type force to obtain best-fit values for the parameters β for different λ. The small size of the measured force combined with

the fact that the thermal noise was comparable to the measured force led them to conclude that their observation is not conclusive evidence for the fact that they observe gravitational interaction. They have also observed that for a complete test of such short range forces, the separation between the test masses (fixed at $25\,\mu$m for their case) needs to be varied. Due to these reasons they use the data to set upper limits on the possible values of the Yukawa strength β for different ranges λ. For a $\lambda \sim 10\,\mu$m they obtain $\beta \sim 10^4$. As Ref.[23] observe, one significant advantage of using an atomic system like Ref.[28] or the proposal we make in this thesis, comes from the fact that one can directly probe very short length scales that are relatively tough to probe using macroscopic systems that were discussed above.

The different experimental papers discussed in this section put our proposal in perspective. In the next section a rough schematic of our setup is discussed and in light of the above experiments the issues that could be important in a practical realisation of the proposal are examined.

5.3 Experimental Schematic

We have in Fig. 5.4, a sketch of the schematic for our proposal. We consider one dimensional dynamics of a single cold atom in a fiber optic cavity. The cavity is created by using a pair of optical fibers, each with an integrated Bragg reflector (the cavity configuration is described in [45]). The driving laser which sustains the electromagnetic mode in the cavity enters through one of the fibers. The other fiber passes through a hole drilled into a disc (uniform otherwise), made of a dense material like gold, and the fibers are aimed at each other with a small gap in between; this gap will act as the cavity. The signal from the cavity is collected at a detector placed below the fiber that passes through the source mass. By using a beam splitter, as shown in the schematic, we use part of the incoming laser signal as the local oscillator that is compared to the signal. Although there are more loss sources from the open cavity setup (we have not included such losses in our idealised theoretical model discussed in the previous chapters), it has the advantage that it is easy to build and the mode structure can be analysed readily (see the Appendix in [45]). The fiber core has a diameter of $5\,\mu$m and the gap between the bragg reflectors is of the order of $L \sim 10^{-2}$ m. The gap between the fibers for the value of κ (cavity linewidth) and g_0 (the dipole coupling constant) we used in our simulations, comes out as $2l \sim 1.563\,\mu$m. The radius of the fiber core is $5\,\mu$m and the waist size of the mode is on the order of 1-2 μm.

The source mass has a thickness of $t_0 \sim 10\,\mu$m and has a radius much greater than the radial extent of the cavity. So the newtonian gravitational field at the cavity, which is assumed to be along the axis, due to a disc can be calculated as follows. Call the distance

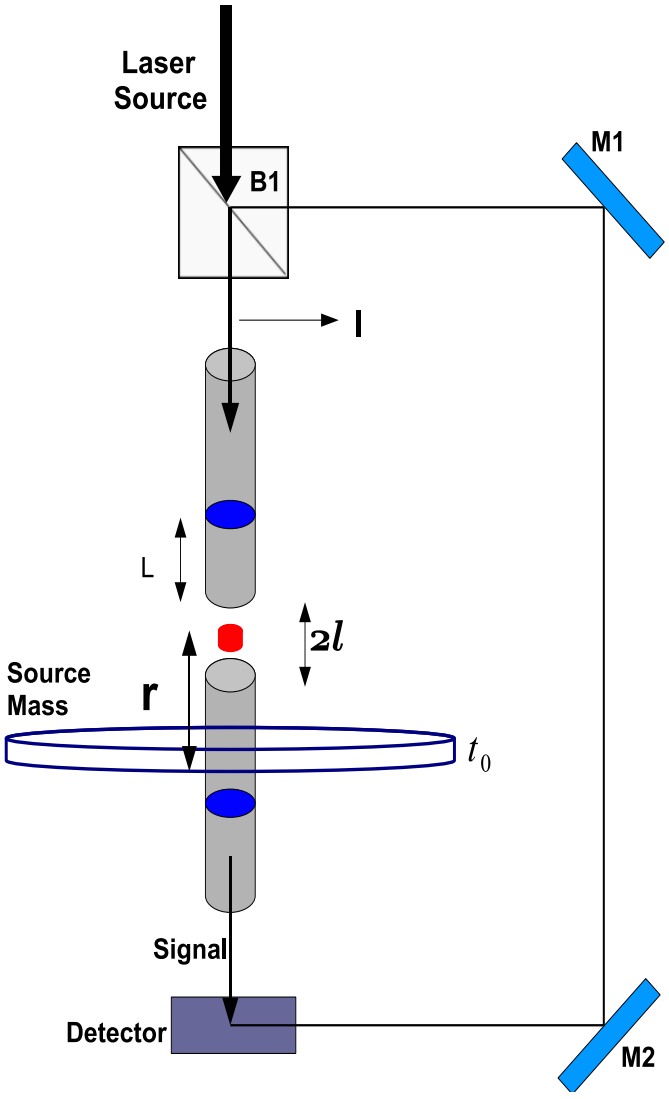

Figure 5.4: Schematic of the proposed experiment, I-incident laser beam; B1 beam splitter, M1 and M2-mirrors, $t_0 = 10\,\mu$m-source mass thickness, r-atom-source mass separation $\sim \mu$m, $2l \sim 1.5\,\mu$m- size of the gap between the fiber ends/cavity length, $L \sim 10^{-2}$ m-distance between the bragg reflectors inside the fiber and the fiber ends.

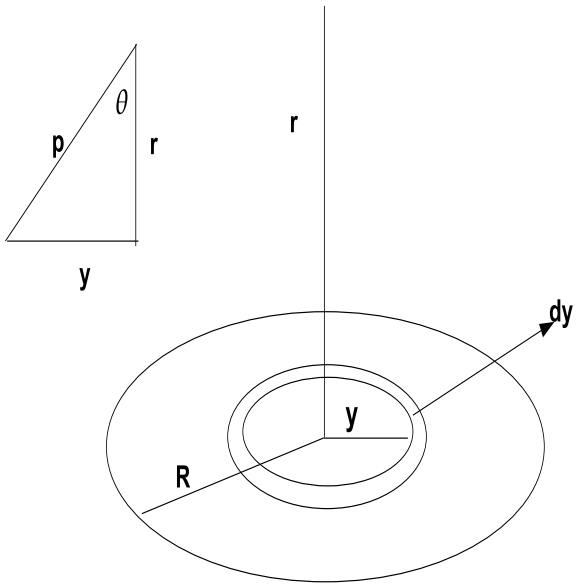

Figure 5.5: Gravitational field along the axis of an uniform disc.

between the disc and the cavity r and the radius of the disc R. For a uniform disc (we will account for the hole through which the fiber passes later), the Newtonian field can be written as an integral over concentric rings. The surface mass density of the disc is given by $\sigma = \rho t_0$, where the volume density $\rho \sim 20$ g/cc for gold. Referring to Fig. 5.5, we write down the acceleration due to the disc as (due to symmetry all the field will be in the vertical direction) :

$$a = \int_0^R \frac{2\pi G\sigma \cos\theta}{p^2} y\, dy \tag{5.2}$$

$$= 2\pi G\sigma r \int_r^{\sqrt{r^2+R^2}} \frac{dp}{p}. \tag{5.3}$$

We assume that the separation between the source mass and the cavity r ($\sim \mu$m) is much smaller than the radius of the disc R ($\sim$ mm). Therefore the net Newtonian acceleration is given by:

$$a = 2\pi G\rho t_0 - \frac{2\pi G\rho t_0 r}{R}. \tag{5.4}$$

The first term is the gravitational field due to an infinite disc. In the limit $R \gg r$, the second term is negligible. The presence of a hole in the disc will reduce this field. The radius of the hole is $\epsilon \sim 5\,\mu$m (radius of the fiber core). From the second term of Eq. 5.4, we can see that the contribution of a finite disc goes as the inverse of its radius. Thus, the relative contribution of the missing piece due to the hole goes as $\epsilon/R \sim 10^{-9}$, which is very small. For the gravitational field due to a finite disc, at a point not on the axis, we refer to [63]. We assume that the Newtonian field due to the disc at the cavity is given by the first

term in Eq. 5.4 for the rest of the discussion.

For $t_0 \sim 10\ \mu$m and $\rho \sim 20$ g/cc (e.g. gold or tungsten), the Newtonian gravitational acceleration is $a \sim 10^{-10}\,\mathrm{ms}^{-2}$. The spatial extent of the (delocalised) atom along the cavity axis is set by the number of sites it occupies in the periodic potential. We have assumed this is on the order of 40 sites in our simulations giving a extent on the order of $10^{-1}\,\mu$m. Hence, r can be defined as the separation between the atomic center of mass in the cavity and the source mass. We choose $r \sim 10\,\mu$m. By measuring the Bloch frequency for different values of r we can determine if there is a deviation from the Newtonian gravity values that we expect from the earlier calculations. These deviations can be modelled using the Yukawa form (Eq. 5.1) and this experiment will provide a direct check on the upper limits of the parameters β and λ set by earlier cantilever experiments [61, 62]. In our simulations, we used a vertically oriented cavity and the only force was gravity given by $F = Mg$. In the experiment the cavity can be oriented in two ways. When vertically oriented, the force due to the source mass will appear as a correction to the Bloch frequency due to gravity (see from above that $a \ll g$). The presence of a large background force like earth's gravity can improve the sensitivity of the experiment as pointed out in the end of last section [29]. Another possible orientation for the cavity is in the horizontal direction where the only force will be that due to the source mass.

The next challenge for the experiment is to load a single atom into the cavity. Trapping a single atom in a high finesse cavity has been achieved by [65] and [64]. As previously noted in Chapter 4, extremely high finesse cavities would affect the adiabaticity arguments where it is assumed that the cavity bandwidth κ is larger than the Bloch frequency. Hence cavity finesse, which determines κ, has to be chosen suitably. The basic idea in such a process will be to first create a source of cold atoms, generally in a MOT trap. This will then drop atoms into the cavity at very slow speeds so that at most one atom passes through the cavity at a given time. In [65] they used a novel feedback technique to increase the intensity of the cavity mode when an atom passes by and this in turn helps to hold the atom in the cavity (they obtain approximate trapping times of 0.25 ms with this technique). The cavity bandwidth used in [65] is $\kappa = 2\pi \times 1.4\,\mathrm{MHz}$ which is of the same order of magnitude as the value we used in our numerical simulations. Another method to load atoms into a cavity is by building a "conveyor belt" made of light (i.e. a moving optical lattice) for atoms that carries them into the cavity. This has been described in the paper by D.Schrader *et al.*, [66] .

There are two important advantages that this proposal has in comparison to the experiments discussed in the last section. The first advantage is the fact that since one is in a single atom situation broadening of the momentum distribution due to interactions is not an issue

(although interaction effects can be suppressed by using degenerate Fermionic atoms, the momentum spread of the degenerate gas, $2\hbar k_F$ is not negligible). The next key advantage is that destructive imaging of the atom to observe BZO is not needed. The observable in our case is the transmitted light from the cavity. The measurement scheme we propose is continuous. This means we can perform a frequency measurement to high accuracy. This is very different from the ballistic expansion measurements where the experiment has to be re-run for each data point.

Although the continuous measurement process in principle will allow the observation of a large number of BZO, in practice we expect incoherent scattering of photons, that can knock the atom out of the cavity, to limit the observation time. Apart from the incoherent scattering event that can kick the atom out of the cavity, the momentum diffusion of the atom can cause heating which will also affect the signal. The fluctuating nature of the dipole force on the atom and the quantum nature of the field manifested by spontaneous emission of photons are sources of diffusion for an atom in a standing wave light field independent of the cavity [67]. The dissipative nature of the cavity (as seen from the linewidth κ) gives an extra source of diffusion [68]. One future direction of our research is to understand diffusion in an optical cavity and estimate its impact on our proposal.

We next estimate the scattering rate due to spontaneous emission. Comparing the atomic recoil momentum due to this scattering event with other relevant momenta in the problem will give an idea of the effect of an emission event. To this end consider first the recoil momentum,

$$p_R = \hbar k_L = \hbar k_c \tag{5.5}$$

where k_c, the cavity mode wave vector, is equal to k_L, since the driving laser and the cavity mode are on resonance. Now the periodicity of the potential is given by $V(x+d) = V(x)$ with $d = \frac{\pi}{k_c}$ and thus the width of a Brillouin zone is :

$$k_{\mathrm{BZ}} = 2k_c. \tag{5.6}$$

Another important momentum scale is the width of the wave function in momentum space. Consider the initial wave function, which in the theoretical analysis of the previous chapters is taken to be a Bloch function. For a Bloch function $\chi_q(x)$ with quasi-momentum index q, the quasi-periodicity (i.e. we can write $\chi_q(x) = e^{iqx}u_q(x)$ such that $u_q(x+d) = u_q(x)$) implies that the Fourier expansion can be written as :

$$u_q(x) = \sum_K c_{q+K} e^{iKx}, \tag{5.7}$$

where the only non-zero Fourier coefficients occur at intervals of K, the reciprocal lattice vector, which is of the same length as the Brillouin zone. Hence the width of the wave function for the lattice depths we consider is at least $K = k_{\mathrm{BZ}} = 2k_c$ (in fact for the lattice depths we consider the width is of the order of $2k_c$).

Comparing equations Eq. 5.5 and Eq. 5.6 we see that the recoil momentum is of the same order of magnitude as the other momentum scales in the problem. This means a single spontaneous emission event can affect the system significantly. Let us now estimate the scattering rate for the parameters we chose in the simulations. The scattering rate for the spontaneous emission process is given by (Eq. $V.C.11$ in Cohen-Tannoudji's book [34])

$$\Gamma_{sc} = \Gamma \sigma_{22}^{st} \tag{5.8}$$

where σ_{22}^{st} is the steady population of the excited state and Γ is the spontaneous decay coefficient. Substituting the value of σ_{22}^{st} we get

$$\Gamma_{sc} = \Gamma \frac{\Omega_1^2}{4\left(\delta^2 + \Gamma^2/4 + \Omega_1^2/2\right)} \tag{5.9}$$

The Rabi frequency Ω_1 is related to the single photon dipole coupling g_0 and the mean photon number in the cavity $\alpha^*\alpha$, by $\Omega_1^2 = 4g_0^2 N = 4g_0^2\alpha^*\alpha$ (Eq. $VI.B.18$ in [34]). The order of magnitude of Ω_1 for our parameters is 10^7 and Γ is of the order of 10^6 whereas the detuning δ is of the order of 10^{10}. Thus smaller terms in Eq. 5.9 can be neglected and the expression simplifies to :

$$\Gamma_{sc} \approx \Gamma \frac{g_0^2 N}{\delta^2}. \tag{5.10}$$

Substituting the values used in the simulations, $\Gamma_{sc} \sim 1.3$ and the number of Bloch oscillations that can be observed before this time scale becomes important is :

$$n = \Gamma_{sc}^{-1}/T_B \approx 600.$$

Note that the above number is very specific to the parameters of the simulations. It should be possible to find a suitable parameter regime (in some of the experiments the values of Γ_{sc} was on the order of 10 s) so that this number is larger.

Since we are making a precision measurement of the gravitational force, the effect of other stray sources must be reduced or eliminated. Such sources include surface forces due to the source mass (like the Casimir Polder force discussed in the last section) and intensity gradients along the axial direction in the standing wave field. One way to take care of such forces is to perform the experiment with different isotopes of the same atom. In this manner

one can account for the stray forces which are mostly electromagnetic in nature. The effect of electromagnetic surface forces can also be reduced by using conductive screens [61, 62]. We expect the size and thickness of this conductive screen to limit the separation r between the source mass and the atom. The exact limits will be investigated as part of future research. The position dependence of some of the extra forces can be used to make them relatively weaker than the force that is being measured (for instance the Casimir Polder force goes as r^{-7}).

One more aspect of the experimental setup that can affect the momentum space distribution of the atom is the intensity and frequency noise of the laser source. The bandwidth of our signal is set by the cavity line width κ. For our simulations, $\kappa = 2\pi \times 0.59 = 3.7\,\mathrm{MHz}$. The signal to be measured has the oscillation frequency $\omega_{\mathrm{B}} \sim 1\,\mathrm{KHz}$. The first thing is to observe is that the signal varies more slowly compared to the bandwidth of the signal, which is usually the case. The next thing is to compare this to the spectrum of the laser intensity noise. The lowest intensity noise possible is set by the inherent Poissonian nature of the photon spectrum and is called shot noise. In addition to shot noise, the general structure of intensity noise [69] for a diode laser shows peaking at lower frequencies ($\nu \leq 500\,\mathrm{kHz}$), for a range of intermediate frequencies ($500\,\mathrm{kHz} < \nu < 3\,\mathrm{GHz}$) there is a broad plateau which rises to a peak at the laser's relaxation frequency (around $2-3\,\mathrm{GHz}$). For frequencies above the relaxation frequency the noise decreases towards the shot noise limit. The laser frequency noise has a spectrum similar to the intensity noise spectrum. The signal frequency to be observed is of the order of a few kHz, which means it is in a range where the intensity noise generally peaks. The bandwidth of the signal (order of MHz) sits in the intermediate ranges of the intensity noise spectrum where there is a plateau. The above discussion is very elementary and gives an idea of the different frequencies involved. The best choice of parameters that minimise the signal to noise ratio are beyond the scope of this thesis and will be reserved for future research. We will also examine which of the two regimes, large or small $g_0^2/(\delta\kappa)$, is ideal to get a good signal to noise ratio. The detection techniques for the regimes will also be different, since one of them involves a phase measurement and the other, an intensity measurement.

This completes a discussion of the experimental setup needed to test the predictions of our theoretical proposal.

Chapter 6

Summary

In Chapter 1, the system under consideration was introduced. The aim is to use BZO of a single cold atom in an optical cavity, to make a precision measurement of gravity. The small size and high sensitivity of the atomic probe would help in detecting deviations from the Newtonian law at micrometer scales. The observable for our proposal is the light transmitted out of the cavity. This makes it different from other cold atom systems used to probe BZO, since destructive imaging techniques used to probe the atoms are not needed, and a continuous measurement of the observable over many oscillations should be possible.

In Chapter 2, the Hamiltonian for the system was presented. The cavity mode is far-detuned from the atomic transition frequency. This means the excited state of the atom can be adiabatically eliminated. The net result is we have a set of coupled equations for the ground state wave function of the atom and the single-mode cavity field. The equation of motion for the wave function (Eq. 2.26a) is a Schrödinger equation for a particle in a periodic potential with an additional constant force. The constant force of interest is $F = Mg$ where g is acceleration due to gravity. The equation of motion for the field (Eq. 2.26b) depends on the atomic degrees of freedom through the coupling integral (Eq. 2.27) which is essentially the atomic expectation value of the periodic potential.

In Chapter 3, the basic theory of BZO was discussed. The periodic semiclassical evolution of the quasi-momentum in the lowest band under the influence of the force term was used to define the Bloch period. A quantum mechanical interpretation of the same was given from the Schrödinger equation obeyed by the gauge transformed wave function (Eq. 3.21). The Houston solution (Eq. 3.25) is the adiabatic solution to the full Hamiltonian. The adiabaticity conditions are summarized by requiring the Bloch frequency ω_{B} to be smaller than other frequencies in the problem (ω_{ho}, Δ_E, κ). It was also noted that the Houston solution can be extended to a case where the lattice depth is modulated with time provided the frequency of modulation is still consistent with the adiabatic condition.

In Chapter 4, the coupled equations of motion were solved. The value of the coupling constant $g_0^2/(\delta\kappa)$ gave two qualitatively different regimes for the solution. When $g_0^2/(\delta\kappa) << 1$, the amplitude of the field was a constant, whereas the phase was modulated at the Bloch frequency. For $g_0^2/(\delta\kappa) \sim 1$, the amplitude of the field was also modulated at the Bloch frequency and we had a situation where the atom moves in a periodic potential and at the same time affects the amplitude of the potential by back-action. A self-consistent solution for the lattice depth was calculated using the adiabatic Houston wave function. This agreed well with the numerically calculated lattice depth. Finally, the higher frequency oscillations found in the lattice depth as a function of time were identified as higher band effects.

In Chapter 5, experiments that studied BZO of cold atoms in optical lattices were discussed. This helped to put our proposal in perspective, and to identify some issues that will be relevant for the experimental realisation. In the last section of Chapter 5 a schematic experimental implementation of the proposal was presented. The spontaneous scattering rate, which limits the number of BZO that can be observed, was calculated. Other sources that can broaden the momentum space distribution were discussed. Future directions of research include an estimation of the right parameter ranges for the experimental realisation, determination of the regime of $g_0^2/(\delta\kappa)$ ($\gg 1$ or $\ll 1$) which is ideal for an experiment and a detailed study of momentum diffusion in an optical cavity.

Appendix A

Adiabatic Elimination

In this appendix we will work out the effective hamiltonian from the original hamiltonian Eq. 2.18. The treatment of the book [31] is closely followed.

Since adiabatic elimination involves only the atom-light interaction term (Eq. 2.12), other terms in the hamiltonian (Eq. 2.18) can be ignored for now. The hamiltonian under consideration is :

$$H_1 = \frac{\hbar\omega_0}{2}\sigma_z + \hbar\omega_c \hat{a}^\dagger \hat{a} + \hbar g_0 \cos(k_c z)\left(\hat{a}\sigma_+ + \hat{a}^\dagger\sigma_-\right)$$

Consider a state for the atom and the light field inside a cavity given by :

$$\mid \psi\rangle = a \mid e\rangle \mid n-1\rangle + b \mid g\rangle \mid n\rangle. \tag{A.1}$$

where $\mid e\rangle$ and $\mid g\rangle$ denote the excited and ground states of the two-level atom respectively and $\mid n\rangle$ denotes the photon number state of the field i.e. $\hat{a}^\dagger\hat{a} \mid n\rangle = n \mid n\rangle$. Substituting the above state into the time dependent Schrödinger equation we get the following equations for a and b :

$$\mathrm{i}\hbar\frac{da}{dt} = \left(\hbar\omega_c(n-1) + \frac{1}{2}\hbar\omega_0\right)a + \hbar g_0\cos(k_c z)b \tag{A.2a}$$

$$\mathrm{i}\hbar\frac{db}{dt} = \left(\hbar\omega_c n - \frac{1}{2}\hbar\omega_0\right)b + \hbar g_0\cos(k_c z)a. \tag{A.2b}$$

Now perform a frame change for the Hamiltonian i.e. apply an unitary transform on the hamiltonian.
Under a general unitary transform U, the hamiltonian H goes to H' as :

$$H' = \mathrm{i}\hbar\dot{\hat{U}}\hat{U}^\dagger + \hat{U}H\hat{U}^\dagger \tag{A.3}$$

The state vector transforms under the same as $\mid \psi_1\rangle = \hat{U} \mid \psi\rangle$. Now let us perform the above unitary transform on H_1 with $U = \mathrm{e}^{\mathrm{i}H_0 t/\hbar}$ where,

$$H_0 = \frac{\hbar\omega_0}{2}\sigma_z + \hbar\omega_c \hat{a}^\dagger \hat{a}. \tag{A.4}$$

The state $\mid \psi_1\rangle$ is transformed as :

$$\mid \psi_2\rangle = \hat{U} \mid \psi\rangle = a_2 \mid e\rangle \mid n-1\rangle + b_2 \mid g\rangle \mid n\rangle \ , \tag{A.5}$$

where the coefficients a_2 and b_2 are given by :

$$a_2 = a\mathrm{e}^{\mathrm{i}[(n-1)\omega_c + \frac{\omega_0}{2}]t} \tag{A.6a}$$

$$b_2 = b\mathrm{e}^{\mathrm{i}[(n)\omega_c - \frac{\omega_0}{2}]t}. \tag{A.6b}$$

The Schrödinger equation in the new frame leads to the following equations for the coefficients :

$$\frac{da_2}{dt} = -\mathrm{i}g_0 \cos(k_c z)\sqrt{n}\,\mathrm{e}^{\mathrm{i}(\omega_0-\omega_c)t} b_2 \tag{A.7a}$$

$$\frac{db_2}{dt} = -\mathrm{i}g_0 \cos(k_c z)\sqrt{n}\,\mathrm{e}^{-\mathrm{i}(\omega_0-\omega_c)t} a_2. \tag{A.7b}$$

To make the final equations for a_2 and b_2 time independent, we need $a_2 \approx \mathrm{e}^{\mathrm{i}(\omega_0-\omega_c)t}$. We derive this by the following procedure. Integrating the equation for $a_2(t)$ we get :

$$a_2(t) = \int_{-\infty}^{t} -\mathrm{i}g_0 \cos(k_c z)\mathrm{e}^{\mathrm{i}(\omega_0-\omega_c)t}\sqrt{n} b_2(\tau) d\tau \tag{A.8}$$

$$= \left[\frac{-\mathrm{i}g_0 \cos(k_c z)}{\mathrm{i}(\omega_0-\omega_c)}\mathrm{e}^{\mathrm{i}(\omega_0-\omega_c)\tau}\sqrt{n} b_2(\tau)\right] - \int_{-\infty}^{t} d\tau\sqrt{n}\left(\frac{\partial b_2}{\partial \tau}\right)\left(\frac{-\mathrm{i}g_0 \cos(k_c z)}{\mathrm{i}(\omega_0-\omega_c)}\mathrm{e}^{\mathrm{i}(\omega_0-\omega_c)\tau}\right). \tag{A.9}$$

For large detuning the ground state population is more or less constant (low excitation probability), which means the factor $\frac{\partial b_2}{\partial \tau}$ varies more slowly in comparison to the exponential term $\mathrm{e}^{\mathrm{i}(\omega_0-\omega_c)\tau}$. We pull out $\frac{\partial b_2}{\partial \tau}$ and evaluate it at t. With this approximation the second term in Eq. A.9 goes as $(\omega_0-\omega_c)^{-2}$ because of the $1/(\omega_0-\omega_c)$ factor coming from the integration of the exponential. For large detuning this term is smaller than the first term of Eq. A.9, which goes as $1/(\omega_0-\omega_c)$. Neglecting the second term the expression for $a_2(t)$ gives :

$$a_2(t) \approx \frac{-g_0 \cos(k_c z)}{\omega_0-\omega_c}\mathrm{e}^{\mathrm{i}(\omega_0-\omega_c)\tau}\sqrt{n} b_2(\tau). \tag{A.10}$$

Substituting this in the equation for b_2 we get :

$$\frac{db_2}{dt} = \frac{\mathrm{i}n \mid g_0 \mid^2 \cos^2(k_c z)}{(\omega_0 - \omega_c)} b_2. \tag{A.11}$$

Consider the effective hamiltonian :

$$H_{\text{eff}}^{'} = \frac{\hbar g_0^2 \cos^2(k_c z)\hat{a}^\dagger \hat{a}}{(\omega_0 - \omega_c)} \sigma_z. \tag{A.12}$$

From the Schrödinger equation,

$$\mathrm{i}\hbar \frac{d \mid \psi_2 \rangle}{dt} = H_{\text{eff}}^{'} \mid \psi_2 \rangle \ , \tag{A.13}$$

one can see that the equation obeyed by b_2 is exactly Eq. A.11. So we have found our effective hamiltonian. Reversing the initial frame change and observing that the effective Hamiltonian (a function of σ_z) is invariant under this leads to the adiabatically eliminated Hamiltonian in its final form :

$$H_{\text{eff}} = \frac{\hbar\omega_0}{2}\sigma_z + \hbar\omega_c \hat{a}^\dagger \hat{a} - \frac{\hbar g_0^2 \cos^2(k_c z)\hat{a}^\dagger \hat{a}}{\delta} \sigma_z. \tag{A.14}$$

Appendix B

Adiabaticity Criterion

Consider the wavefunction :

$$\Psi = \sum_n a_n(t) u_{q+2\pi n-\lambda t} \exp\left[\mathrm{i}(q+2\pi n-\lambda t)z\right] \exp\left[-(\mathrm{i}/\hbar)\int^t E_{q+2\pi n-\lambda\tau} d\tau\right]. \tag{B.1}$$

Here the index n is the band-index we mentioned previously. a_n is then the probability amplitude for the wavefunction to be in band n. Substitute this into the Schrödinger Eq. 3.20 and use the orthogonality of the Bloch functions belonging to different zones/bands (we have a complete set of basis functions), we get an equation for the coefficients a_n :

$$\begin{aligned}\frac{da_n}{dt} = \sum_m a_m \left(\int dz u^*_{q+2\pi n-\lambda t}(z)\lambda \frac{du_{q+2\pi m-\lambda t}(z)}{dq} \exp\left[2\pi\mathrm{i}(m-n)z\right]\right) \\ \exp\left[-(\mathrm{i}/\hbar)\int^t \left(E_{q+2\pi m-\lambda\tau} - E_{q+2\pi n-\lambda\tau}\right) d\tau\right].\end{aligned} \tag{B.2}$$

Let us from now denote $u_{q+2npi-\lambda t}$ as $u_{q(t),n}$ making explicit the fact that n is the band index. Now the instantaneous eigenvalue equation for the Bloch function $\phi_{q(t),n}$ leads to an equation for u (Eq. 3.22) :

$$H_u u_{q,m} = \left(\left(\frac{(\hat{p}-\hbar q)^2}{2M}\right) + s\cos^2(k_c z)\right) u_{q,m}(z) = E_{q,n} u_{q,m}(z). \tag{B.3}$$

Differentiating the above equation with respect to q we have :

$$\frac{\partial H_u}{\partial q} u_{q,m} + H_u \frac{\partial u_{q,m}}{\partial q} = E_{q,m}\frac{\partial u_{q,m}}{\partial q} + \frac{\partial E_{q,m}}{\partial q} u_{q,m} \tag{B.4a}$$

$$\frac{-\hbar}{M}\hat{p} u_{q,m} + \frac{\hbar^2 q}{M} u_{q,m} + H_u \frac{\partial u_{q,m}}{\partial q} = E_{q,m}\frac{\partial u_{q,m}}{\partial q} + \frac{\partial E_{q,m}}{\partial q} u_{q,m}. \tag{B.4b}$$

Now when the inner product of the last equation with $u^*_{q,n}\exp\left[2\pi i(m-n)z\right]$, such that $m \neq n$, is taken the following terms drop out due to the orthogonality of the Bloch functions :

$$\int dz u^*_{q,n}\frac{\partial E_{q,m}}{\partial q}u_{q,m}\exp\left[2\pi\mathrm{i}(m-n)z\right]=0 \tag{B.5a}$$

$$\int dz u^*_{q,n}\frac{\hbar^2 q}{M}u_{q,m}\exp\left[2\pi\mathrm{i}(m-n)z\right]=0. \tag{B.5b}$$

One of the terms that occurs as a result of taking the inner product can be rewritten in this manner :

$$\int dz u^*_{q,n}\frac{\partial u_{q,m}}{\partial q}\exp\left[2\pi\mathrm{i}(m-n)z\right]=\frac{1}{E_{q,m}-E_{q,n}}\int dz u^*_{q,n}\frac{-\hbar}{M}\hat{p}u_{q,m}\exp\left[2\pi\mathrm{i}(m-n)z\right]. \tag{B.6}$$

Substituting the last expression Eq. B.6 into the Eq. 3.22 one gets :

$$\frac{da_n}{dt}=\sum_m a_m\left(\int dz u^*_{q+2\pi n-\lambda t}\lambda\frac{-\hbar\hat{p}}{M}u_{q+2\pi m-\lambda t}\exp\left[2\pi\mathrm{i}(m-n)z\right]\right)\frac{1}{E_{q,m}-E_{q,n}} \exp\left[-(\mathrm{i}/\hbar)\int^t\left(E_{q+2\pi m-\lambda\tau}-E_{q+2\pi n-\lambda\tau}\right)d\tau\right]. \tag{B.7}$$

Let us say we start with a Bloch wavefunction with quasi-mometum in the first Brillouin zone ($m=0$) or the lowest band. As this wavefunction evolves and reaches the edge of the first brillouin zone, one can observe two things from equation Eq. B.7. Change in the coefficient a_n is largest for that n which has very small $(E_{q,m}-E_{q,n})$. One quasimomentum vector that satisfies this condition is the one at the opposite edge of the Brillouin zone. Hence this justifies the Bragg scattering idea. Now the strength of the transition amplitude to other bands depends directly on F and inversely on the difference in energy between the bands $(E_{q,m}-E_{q,n})$ as one can observe from Eq. B.7. Thus this shows that with sufficiently deep periodic potentials and weak enough forces one can avoid the tunneling to higher bands preserving adiabaticity.

The exact condition for adiabatic evolution can be written down by recognising that equation Eq. B.7 gives the rate of change of probability amplitude to occupy higher bands. The adiabaticity criterion requires this rate to be much smaller than the frequency of the energy gap between the bands. Let us say after the adiabatic terms only the first excited band has significant contribution in the RHS of Eq. B.7 and call the energy difference between

ground band and first excited band Δ_E, we have :

$$\frac{\hbar\lambda\langle u_{q,m} \mid \hat{p} \mid u_{q,n}\rangle}{M\Delta_E} << \Delta_E/\hbar \tag{B.8a}$$

$$\hbar\omega_{\mathrm{B}} << \frac{M\Delta_E^2 d}{\hbar\langle u_{q,m} \mid \hat{p} \mid u_{q,n}\rangle} \ , \tag{B.8b}$$

where $\omega_{\mathrm{B}} = Fd/\hbar$ is the Bloch frequency. Now near the edge of the band one can model the lower and higher band as almost degenerate plane waves with momenta given by the field momenta k_c. Thus, the final expression for the adiabaticity criterion is :

$$\hbar\omega_{\mathrm{B}} << \frac{M\Delta_E^2 d}{\hbar^2 k_c}. \tag{B.9}$$

Bibliography

[1] C. Zener, Proc. R. Soc. A **145**, 523 (1934)

[2] F. Bloch, Z. Phys. **52**, 555 (1928)

[3] J. Feldmann *et al.*, Phys. Rev. B **46**, 7252 (1992); C.Waschke *et al.*, Phys. Rev. Lett. **70**, 3319 (1993)

[4] J. P. Reynolds and M. Luban, Phys. Rev. B **54**, R14301 (1996)

[5] M. Ben-Dahan *et al.*, Phys. Rev. Lett. **76**, 4508 (1996)

[6] B. P. Anderson and M. A. Kasevich, Science **282**, 1686 (1998)

[7] D. J. Wineland, H. G. Dehmelt, Bull. Am. Phys. Soc. **20**, 637 (1975); T. W. Hänsch, A. L. Schawlow, Opt. Comm. **13**, 68 (1975); V. S. Letokhov, V. G. Minogin, B. D. Pavlik, Opt. Commun **19**, 72 (1976)

[8] D. J. Wineland *et al.*, Phys. Rev. Lett. **40**, 1639 (1978); W.Neuhauser *et al.*, Phys. Rev. Lett. **41**, 233 (1978)

[9] W. I. Balykin, V. S. Letokhov, V. I. Mishin, Pis'ma Zh. Eksp. Teor. Fiz. **29**, 614 (1979); J. E. Bjorkholm *et al.*, Phys. Rev. Lett. **41**, 1361 (1978); Appl. Phys. Lett. **36**, 99 (1980); Opt. Lett. **5**, 11 (1980); S. A. Andreev *et al.*, Pis'ma Zh. Eksp. Teor. Fiz. **34**, 463 (1981); Zh. Eksp. Teor. Fiz. **82**, 1429 (1982); W. P. Phillips, H. J. Metcalf, Phys. Rev. Lett. **48**, 596 (1982); S. Chu *et al.*, Phys. Rev. Lett. **58**, 48 (1985); P. Lett *et al.*, Phys.Rev.Lett **61**, 169 (1988); J. Dalibard and C. Cohen-Tannoudji, J. Opt. Soc. Am. B **6**, 2023 (1989); P. Ungar *et al.*, J. Opt. Soc. Am. B **6**, 2058 (1989)

[10] K. B. Davis *et al.*, Phys. Rev. Lett. **75**, 3969 (1995)

[11] M. H. Anderson *et al.*, Science **269**, 198 (1995)

[12] M. Greiner *et al.*, Nature **415**, 39 (2002)

[13] B. Paredes *et al.*, Nature **425**, 277 (2004)

[14] I. Bloch, J.Phys. B At. Mol. Opt. Phys. **38**, S629 (2005)

[15] I. Bloch *et al.*, Rev. Mod. Phys. **80**, 885 (2008)

[16] C. J. Hood *et al.*, Phys. Rev. Lett. **80**, 4157 (1998)

[17] J. Ye *et al.*, Phys. Rev. Lett. **83**, 4987 (1999)

[18] J. McKeever and H. J. Kimble, in Laser Spectroscopy XIV, eds. S. Chu, V. Vuletic, A. J. Kerman and C. Chin, "Cavity QED With Cold Atoms" (World Scientific, 2002)

[19] G. Rempe, Contemporary Physics **34**, 119 (1993)

[20] G. Rempe, App. Phys. B **60**, 233 (1995)

[21] P. M*ü*nstermann *et al.*, Phys. Rev. Lett. **84**, 4068 (2000)

[22] Nima Arkani-Hamed *et al.*, Phys. Lett. B **429**, 263 (1998)

[23] S. Dimopoulos and A. A. Geraci, Phys. Rev. D **68**, 124021 (2003)

[24] O. Morsch *et al.*, Phys. Rev. Lett. **87**, 140402 (2001)

[25] G. Roati *et al.*, Phys. Rev. Lett. **92**, 230402 (2004)

[26] R. Battesti *et al.*, Phys. Rev. Lett. **92**, 253001 (2004)

[27] P. Cladé *et al.*, Phys. Rev. Lett. **96**, 033001 (2006)

[28] G. Ferrari *et al.*, Phys. Rev. Lett. **97**, 060402 (2006)

[29] I. Carusotto *et al.*, Phys. Rev. Lett. **95**, 093202 (2005)

[30] H. B. G. Casimir and D. Polder, Phys. Rev. **73**, 360 (1948)

[31] Quantum Optics, D. F. Walls and G. J. Milburn, Springer-Verlag (1994)

[32] Elements of Quantum Optics, P. Meystre and M. Sargent III, Springer (1997)

[33] K. S. Wong et.al., Opt. Comm. **137**, 269 (1997)

[34] C. Cohen-Tannoudji, J. Dupont-Roc and G. Grynberg, Atom-Photon Interactions (Wiley-Interscience,1998)

[35] Igor. B. Mekhov *et al.*, Phys. Rev. A **76**, 053618 (2007)

[36] Solid State Physics, N. W. Ashcroft and N. D. Mermin, Holt, Rinehart and Winston, New York (1988)

[37] M. Holthaus and D. W. Hone, Phil. Mag. B, **74**, No:2, 105 (1996)

[38] W. V. Houston, Phys. Rev. **57**, 184 (1942)

[39] G. H. Wannier, Phys. Rev. **117**, 432 (1960); Rev.Mod.Phys. **34**, 645 (1962)

[40] J. Zak, Phys. Rev. Lett **20**, 1477 (1968); Phys.Rev. **181**, 1366 (1969)

[41] A. Rabinovitch and J. Zak, Phys. Rev. B **4**, 2358 (1971); Phys.Lett. **40A**, 189 (1972)

[42] G. H. Wannier, Phys. Rev **181**, 1364 (1969)

[43] G. Nenciu, Rev. Mod. Phys **63**, 91 (1991)

[44] Image adapted from the lecture notes in `http://physics.valpo.edu/courses/p440/`

[45] Peter Horak *et al.*, Phys. Rev. A **67**, 043806 (2003)

[46] MATLAB is a registered software with The MathWorks, Inc., Natick, MA (1998)

[47] Expokit. A Software Package for Computing Matrix Exponentials, Sidje R. B., ACM Trans. Math. Softw., 24, 130-156

[48] Wolfram Research, Inc., Mathematica, Version 5.2, Champaign, IL (2005)

[49] Quentin Thomenn *et al.*, J. Opt. B:Quantum Semiclass. Opt. **6**, 301 (2004)

[50] A. M. Bouchard and Marshall Luban, Phys. Rev. B **52**, 5105 (1995)

[51] Pavel Abumov and D. W. L. Sprung, Phys. Rev. B **75**, 165421 (2007)

[52] E. Raab *et al.*, Phys. Rev. Lett. **59**, 2631 (1987)

[53] W. Petrich *et al.*, Phys. Rev. Lett. **74**, 3352 (1995)

[54] P. Maunz *et al.*, Nature **428**, 50 (2004)

[55] D. Choi and Q. Niu, Phys. Rev. Lett. **82**, 2022 (1999)

[56] G. H. Wannier, Phys. Rev. **117**, 432 (1960)

[57] http://www.ngs.noaa.gov/GRD/GRAVITY/ABSG.html

[58] Proceedings of the JH Workshop, Firenze, 2001, edited by I. Ciufolini *et al.* (World Scientific, Singapore, 2003); G. M. Tino, Nucl. Phys. B (Proc. Suppl.) **113**, 289 (2002)

[59] D. M. Harber *et al.*, Phys. Rev. A **72**, 033610 (2005)

[60] J. C. Long and J. C. Price, Comptes Rendus Physique **4**, 337 (2003)

[61] J. C. Long *et al.*, Nature (London) **421**, 922 (2003)

[62] S. J. Smullin *et al.*, Phys.Rev. D **72**, 122001 (2005)

[63] F. T. Krogh *e al.*, Celestial Mechanics **26**, 395 (1982)

[64] J. Ye *et al.*, Phys. Rev. Lett **83**, 4987 (1999)

[65] P. W. H. Pinkse *et al.*, Nature **404**, 365(2000)

[66] D. Schrader *et al.*, Appl.Phys.B **73**, 819 (2001)

[67] J. P. Gordon and A. Ashkin, Phys. Rev. A **21**, 1606 (1980)

[68] P. Horak et.al, Phys. Rev. Lett. **79**, 4974 (1997)

[69] C. E. Wieman and L. Hollberg, Rev. Sci. Instrum. **62**, 1 (1991)